[American Journal of Science, Vol. 318, September, 2018, P. 727–763, DOI 10.2475/07.2018.01]

American Journal of Science

SEPTEMBER 2018

RELATING SOIL GAS TO WEATHERING USING ROCK AND REGOLITH GEOCHEMISTRY

GARY E. STINCHCOMB[*,**,†], HYOJIN KIM[*], ELIZABETH A. HASENMUELLER[*,***], PAMELA L. SULLIVAN[*,§], PETER B. SAK[§§,*], and SUSAN L. BRANTLEY[*]

ABSTRACT. **Weathering-induced fracturing (WIF) has been posited to be a mechanism that develops secondary porosity when mineral reaction fronts separate over depth intervals in regolith, and, in particular, when oxidation (which can promote porosity development through volume expansion) occurs deeper than dissolution (which grows porosity through material removal). If this is true, then the protolith's capacity to reduce O_2 [for example, the Fe(II) content] and O_2 availability should affect WIF. This study explores the hypothesis that if the ratio of pO_2 to pCO_2, in soil water, $R'_{(aq)}$, is greater than the ratio of the capacity of the protolith to consume O_2 and CO_2, R^0, then WIF is more likely to occur, and regolith will become thicker. We evaluated this hypothesis by measuring the bulk geochemistry of regolith and rock and monitoring soil gas at three sites, encompassing a wide range of FeO concentrations and regolith thickness: a Pennsylvania (PA) diabase (10.15%; 3.8 m), a Virginia (VA) diabase (10.49%; 1.4 m), and a VA granite (1.45%; 20 m). We inferred soil water O_2 concentrations from calculated equilibrium with the measured soil gas pO_2. We observed WIF in the VA granite and PA diabase where $R'_{(aq)} > R^0$, while at the site that lacked WIF – the VA diabase – $R'_{(aq)} < R^0$, particularly during the wet season. In the VA diabase, the presence of swelling clays (smectite) limits the ability of the oxidant (O_2) to diffuse deeper into the weathering profile during the wet season and microbially accelerated iron oxidation rapidly consumes O_2, limiting O_2 availability for WIF. Smectite has little to no observable effect on O_2 consumption in the PA diabase because the PA diabase is more fractured. A compilation of dissolved soil gas oxidation ratios, the stoichiometric ratio of O_2 consumed to CO_2 produced, shows that for unsaturated conditions, the mean is -1.45 ± 0.88, which is consistent with aerobic root and microbial respiration and the oxidation of organic matter. For near-saturated conditions, the mean oxidation ratio of the compilation is -3.46 ± 1.79, which is consistent with Fe redox and microbial metabolism under reducing conditions. The consistency between the VA and PA data presented here and the compilation suggests that soil water surplus drives coupled Fe-redox reactions that may act as a negative feedback, limiting O_2 supply and WIF under wetter soil moisture conditions.**

We defined Rz, the ratio of O_2 consumption to CO_2 consumption during weathering for each depth interval, z. For all profiles, $R'_{(aq)} > Rz$ near the surface but $R'_{(aq)}$ approaches Rz in the saprolite. We suggest that $R'_{(aq)} > Rz$ in the soil reflects consumption of O_2 and production of CO_2 due to biotic processes whereas $R'_{(aq)}$ approaching Rz suggests that low fluxes at depth are at least partly dictated by rock and regolith composition, notably

* Earth and Environmental Systems Institute, Department of Geosciences, Pennsylvania State University, University Park, Pennsylvania 16802

** Watershed Studies Institute & Department of Earth and Environmental Sciences, Murray State University, Murray, Kentucky 42071

*** Department of Earth & Atmospheric Sciences, Saint Louis University, Saint Louis, Missouri 63108

§ Department of Geography and Atmospheric Science, University of Kansas, Lawrence, Kansas, 66045

§§ Department of Earth Sciences, Dickinson College, Carlisle, Pennsylvania 17013

† Corresponding author: gstinchcomb@murraystate.edu; 270-809-6761

tortuosity of pores. In the VA diabase, we observed $R'_{(aq)} < Rz$ occasionally during the wet season in the lowermost soil and saprolite. Thus, at times the O_2 availability may be less than the O_2 consumption at that depth, consistent with Fe(II) loss and a lack of WIF. Mass-balance calculations show Fe loss in the VA diabase. The influence of rock composition on aqueous O_2/CO_2 concentrations in saprolite is consistent with the hypothesis that the protolith's capacity to consume O_2 and CO_2 has some effect on oxidation and acid consumption deep in the weathering profile.

Keywords: soil, regolith, weathering-induced fracturing, O_2, CO_2, oxidation

INTRODUCTION

As minerals formed at depth equilibrate at Earth's surface during weathering, they undergo redox and acid-base reactions in the presence of O_2 and CO_2, the most important oxidant and acid, respectively. These reactions control atmospheric pCO_2 over tens of thousands to tens of millions of years, acting as negative feedbacks (Ebelmen, 1845; Chadwick and others, 1994; Munhoven, 2002; Berner and others, 2003; Berner, 2006). Thus, measuring and modeling these reactions in regolith gives insight into the C cycle. By generalizing minerals to their oxides, we can explore this concept further. For example, the most abundant redox-active metal in the crust, Fe, oxidizes during weathering as follows:

$$4FeO_{(s)} + O_{2(aq)} \rightarrow 2Fe_2O_{3(s)}, \quad (1)$$

whereas dissolution of the abundant alkali and alkaline metals consumes two moles of CO_2 and one mole of H_2O:

$$Na_2O_{(s)} + 2CO_{2(aq)} + H_2O \rightarrow 2Na^+ + 2HCO_3^-, \quad (2)$$

$$K_2O_{(s)} + 2CO_{2(aq)} + H_2O \rightarrow 2K^+ + 2HCO_3^-, \quad (3)$$

$$MgO_{(s)} + 2CO_{2(aq)} + H_2O \rightarrow Mg^{2+} + 2HCO_3^-, \quad (4)$$

$$CaO_{(s)} + 2CO_{2(aq)} + H_2O \rightarrow Ca^{2+} + 2HCO_3^-. \quad (5)$$

These generalized reactions (eqs 1–5) show that chemical weathering is, in essence, the donation of electrons from rocks to the main electron acceptor, O_2, and the consumption of protons by bases (rocks) near Earth's surface. Weathering in soils reflects these reactions (eqs 1–5) along with the reactions that control soil organic matter like carbon fixation (forward reaction) and oxidation of organic matter as well as root and microbial respiration (reverse reaction):

$$CO_2 + H_2O \leftrightarrow CH_2O + O_2. \quad (6)$$

In a series of papers, Holland and others (Holland, 1978, 1984; Holland and Zbinden, 1988; Pinto and Holland, 1988) showed how pCO_2 and pO_2 in the atmosphere could affect the amounts of pCO_2 and pO_2 in the soil porewater and the extent of leaching of alkali and alkaline earth oxides and FeO in soils on the early, mostly abiotic, Earth. The "abiotic" curves shown in figure 1 were posited based on descriptions of ancient soils formed before biota populated Earth to a significant degree (Holland, 1984; Pinto and Holland, 1988), but with modern ambient pCO_2 and pO_2. Brantley and others (2014) explored how such ideas might be used to understand modern, biotic soils. Based on the small number of published soil gas studies, they documented two types of curves for pCO_2 (that is, biotic i and biotic ii) (fig. 1). In the biotic i curve, pCO_2 increases with depth, reaches an inflection point, and then declines with increasing depth. In contrast, the biotic ii curve shows pCO_2 reaches a maximum value but the concentrations remain more or less constant at deeper depths.

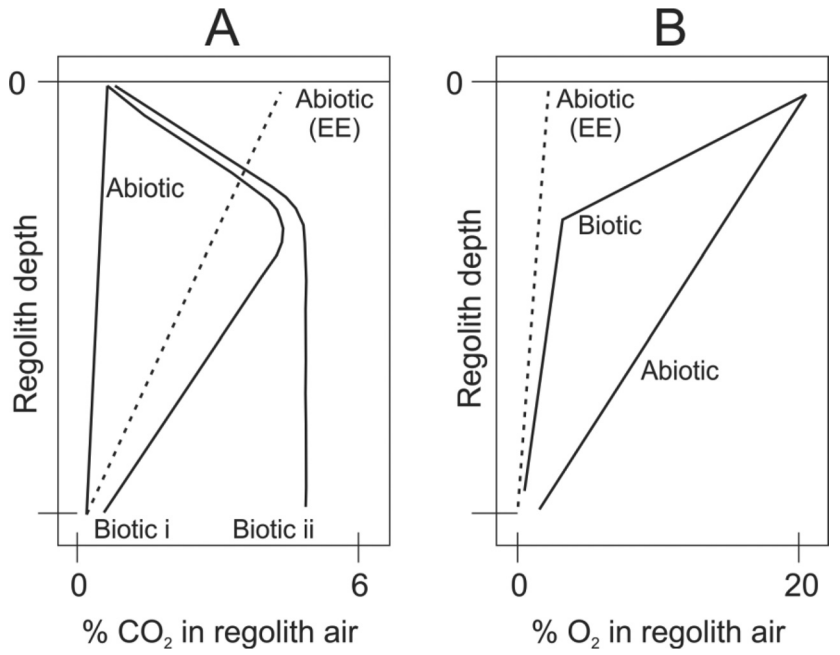

Fig. 1. Schematic diagram (modified from Brantley and others, 2014) showing changes in soil CO_2 and O_2 with depth using modern ambient pCO_2 and pO_2 conditions (solid black lines). "Abiotic" profiles are those with little to no biotic influence and were inferred using Early Earth (EE) conditions (for example, Pinto and Holland, 1988). The abiotic EE conditions (dashed black line) are also shown. Biotic i shows a pronounced decrease in % CO_2 below the maximum % CO_2, whereas biotic ii shows little to no decrease below the maximum.

Both biotic i (Reardon and others, 1979; Fisher and others, 1985; Richter and Markewitz, 1995, 2001; Birkham and others, 2003; Klusman, 2003) and biotic ii (Boynton and Reuther, 1939a; Vine and others, 1943; Zonn and Li, 1960; Amundson and others, 1989; Amundson and Davidson, 1990 and references therein; Davidson and Trumbore, 1995; Birkham and others, 2003) curves have been documented a few times in the literature. In general, the biotic i curve was assumed to reflect downward diffusive flux from the rooting zone combined with CO_2 consumption via weathering.

Modeling (Suchet and others, 2003) and empirical (Bazilevskaya and others, 2013, 2015) results show that lithology impacts the amount of O_2 or CO_2 consumed during weathering and the depth of regolith formation. For example, average regolith thickness on granite is a factor of 20 greater than on diabase in ridge top locations in the Virginia (VA) Piedmont of the eastern United States (Bazilevskaya and others, 2013). These ridge top weathering profiles were considered to be residual soils developed due to top-down infiltration of meteoric waters. The 20-fold discrepancy in regolith thickness was attributed to the difference in fluid transport properties in the weathering granite versus the diabase (Bazilevskaya and others, 2015). In particular, in the mafic diabase, solute transport was inferred to be dominated by diffusion whereas in the felsic granite, it was dominated by advection. In general, the depth interval over which a mineral weathering reaction occurs (the reaction front) is wider where solutes advect rather than diffuse (Brantley and Lebedeva, 2011). Bazilevskaya and others (2015) therefore argued that hydraulic conductivity and the resulting geochemistry of the pore fluids accounted for the difference in regolith thickness.

Key to the argument made by Brantley and others (2014) was the observation that deep infiltration of advecting fluids into the granite was facilitated by the development of secondary porosity through weathering induced fracturing (WIF). Specifically, biotite oxidation was noted to be the deepest reaction in the rock. Such oxidation can cause volume expansion, and it was surmised that this expansion cracks the rock, driving deeper fluid penetration, wider reaction fronts, and formation of deeper regolith. Brantley and others (2014) argued that the ratio of the initial capacity of the rock to consume O_2 versus CO_2, R^0 (as originally defined by Holland), was an important determinant in whether WIF occurred, which in turn allowed deeper regolith to form (see table 1 for glossary of variables). Specifically, R^0 differed for Fe-poor granite ($R^0 = 0.02$) versus Fe-rich diabase ($R^0 = 0.04$), affecting the capacity to consume O_2 (eq 1) and determining whether WIF occurred. Brantley and others (2014) assumed that the regolith atmosphere gas concentrations were the same for the two lithologies, and that O_2 would be consumed at a shallower depth on the Fe-rich diabase than the Fe-poor granite. Without deep oxidation, WIF therefore did not occur on the diabase but did occur on the granite, explaining the deep regolith on the felsic rock. Brantley and others (2014) pointed to evidence in the literature that the oxidation of biotite and its eventual transformation to vermiculite opened up the permeability of rock, driving fluid flow and deeper depths of weathering (Pavich and others, 1989; Buol and Weed, 1991; Graham and others, 1994; Bazilevskaya and others 2013, 2015; Brantley and others, 2013; Navarre-Stichler and others, 2015).

In Brantley and others (2014), observations about regolith depth were made for two profiles in the VA Piedmont in the context of the Holland formulation, but no soil gas data were available for the case studies. Additionally, very few studies examine soil gas at depths below the maximum observed pCO_2 (Richter and Billings, 2015). Here, we return to the granitic and diabase interfluves in the VA Piedmont and explore the recent measurements of pO_2 and pCO_2 for these rocks (Kim and others, 2017). Given that Bazilevskaya and others (2013) had concluded that the presence or absence of fractures due to WIF was a controlling factor for the 20-fold difference in regolith thickness on the granite and diabase, we also analyzed a more fractured diabase profile developed 160 km to the north in Pennsylvania (PA) that was known to have experienced WIF (Hausrath and others, 2011). Weathering of each of the three interfluves has been the subject of previous work (Pavich and Obermeier, 1985; Pavich and others, 1985; Pavich and others, 1989; White and others, 2001; Hausrath and others, 2011; Moore and others, 2012; Bazilevskaya and others, 2013, 2015; Yesavage and others, 2016) as has the gas chemistry in the three settings (Kim and others, 2017). Using these two lithologies, we investigate the relationship between modern-day soil gas concentrations and the recorded extent of consumption of O_2 and CO_2 during weathering to understand porosity and permeability development and controls on regolith thickness. Soil gas and groundwater data were also compiled from previous work in an attempt to place the observations about gas chemistry versus depth into a broader, landscape scale.

BACKGROUND AND METHODS

Site Description

The PA diabase site is located in the Great Valley section of the Ridge and Valley province near Carlisle, PA, United States. The VA diabase and VA granite sites are both located in the Mesozoic lowlands and Foothills sections, respectively, of the Piedmont province outside of Washington, DC, United States (fig. 2). Currently, the three sites are weathering in humid-continental to humid-subtropical climates under temperate broadleaf forests. The mean annual temperature (MAT) ranges from 10.7 to 12.4 °C and the mean annual precipitation (MAP) ranges from 1,045 mm yr^{-1} to 1,066 mm

TABLE 1

Parameters describing the PA and VA samples

Parameter	Equation	Comment	Units
τ_j	$\tau_j = \frac{C_{j,w}}{C_{j,p}} \frac{C_{i,p}}{C_{i,w}} - 1$	Tracks mobile element additions and losses in an open system.	-
$\varepsilon_i(z)$	$\varepsilon_i(z) = \frac{V_w - V_p}{V_p} = \frac{\rho_p}{\rho_w} * \frac{C_{Ti,p}}{C_{Ti,w}}$ - 1	Tracks closed-system volumetric changes (that is, dilation and collapse) during weathering.	-
$\tau_{FeO}^{oxidized}$	$\tau_{FeO}^{oxidized} = \frac{2\left(C_{Fe_2O_3,w} - C_{Fe_2O_3,p}\right) * C_{i,p}}{C_{FeO,p} * C_{i,w}}$	The fraction of Fe(II) in the parent material that has been oxidized and converted to Fe(III). Does not account for Fe(III) in unweathered rock.	-
$M_{O_2}^0$	$M_{O_2}^0 = 0.25 M_{(FeO)}^0$	Capacity for O_2 consumption in unweathered rock.	mol kg^{-1}
$M_{CO_2}^0$	$M_{CO_2}^0 = 2\Sigma M_{(base\ oxides)}^0$	Capacity for CO_2 consumption in unweathered rock.	mol kg^{-1}
$mO_2\ (z)$	$mO_2\ (z) = \frac{0.25\ C_{FeO,p}\ \tau_{FeO}^{oxidized}(z)}{\varepsilon_i(z) + 1}$	Inferred consumption of O_2 at sample depth, z.	mol g^{-1}
$mCO_2(z)$	$mCO_2\ (z) = \frac{-2\ \Sigma C_{Ca+Na+Mg+K,p}\ \tau_{Na+Mg+Ca+K,w}(z)}{\varepsilon_i(z) + 1}$	Inferred consumption of CO_2 at sample depth, z.	mol g^{-1}
mO_2	$mO_2 = \rho_p \int_0^{L_w} \frac{0.25\ C_{FeO,p}\ \tau_{FeO}^{oxidized}(z)}{\varepsilon_i(z) + 1}\ dz$	Depth-integrated consumption of O_2 over the entire regolith profile.	mol cm^{-2}
mCO_2	$mCO_2 = \rho_p \int_0^{L_w} \frac{-2\ \Sigma C_{Ca+Na+Mg+K,p}\ \tau_{Na+Mg+Ca+K,w}(z)}{\varepsilon_i(z) + 1}\ dz$	Depth-integrated consumption of CO_2 over the entire regolith profile.	mol cm^{-2}
R^0	$R^0 = \frac{M_{O_2}^0}{M_{CO_2}^0} = \frac{0.25 M_{FeO}^0}{2\left(M_{Na_2O}^0 + M_{K_2O}^0 + M_{MgO}^0 + M_{CaO}^0\right)}$	Capacity of unweathered rock to consume O_2 versus CO_2.	-
Rz	$Rz = \frac{mO_2\ (z)}{mCO_2\ (z)}$	The ratio of O_2 to CO_2 consumed in the regolith at depth, z.	-
R	$R = \frac{mO_2}{mCO_2}$	Depth-integrated ratio of O_2 to CO_2 consumption in weathered profile.	-
$R'_{(aq)}$	$R'_{(aq)} = \frac{pO_2 * H_{O2}}{pCO_2 * H_{CO2}}$	Ratio of pO_2 to pCO_2 availability in porewater, assuming equilibrium.	-

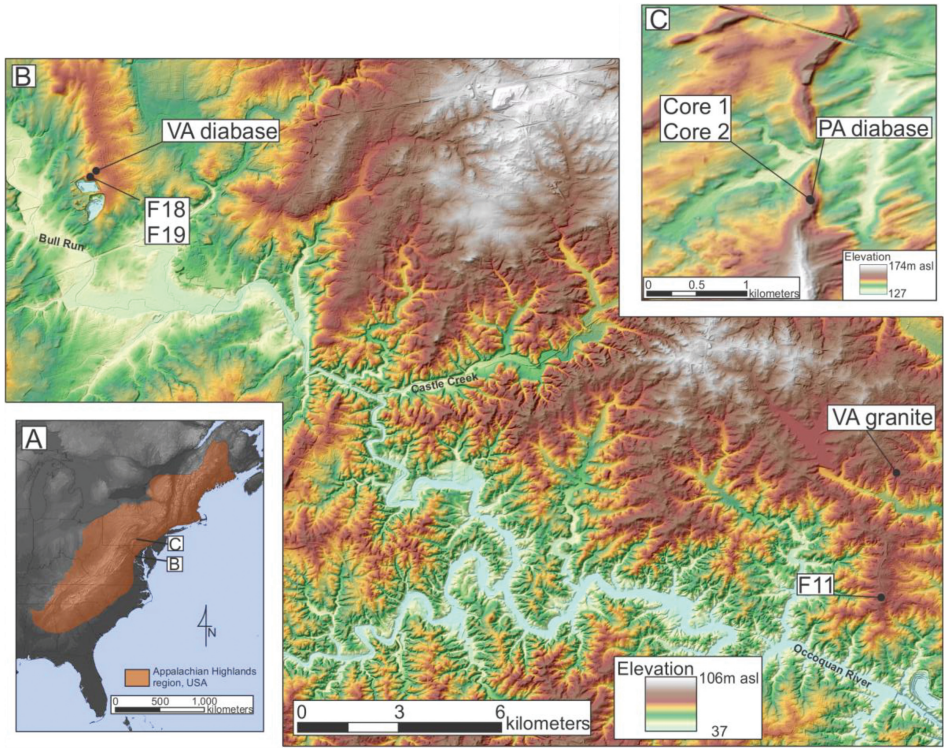

Fig. 2. Study area map showing core and gas sampling locations in (A) the Appalachian highlands region of the northeastern United States. (B and C) Shaded relief map of the VA (B) and PA (C) study areas showing topography of gas sampling sites that are all located along upland interfluves where the hydrology is assumed to be controlled by downward flowing water, that is, 1D profiles (Jin and others, 2010). (B) Location of the VA granite and diabase cores and gas sampling profiles. The VA diabase gas profile is located along the Triassic-Jurassic Manassas diabase sill near Bull Run. The F18 and F19 diabase cores (Pavich and others, 1989; Bazilevskaya and others, 2013, 2015) were collected near the VA diabase. The VA granite gas sampling location is along Cambro-Ordovician Occoquan granite. The F11 granite core's approximate location is the site of previous work (Pavich and others, 1989; Bazilevskaya and others, 2013, 2015) mentioned throughout text. (C) Location of the PA diabase gas sampling profile, located along a narrow ridge of Triassic-Jurassic diabase dike intruding Ordovician limestone country rock. Cores 1 and 2 are regolith profiles from previous work (Hausrath and others, 2011; Yesavage, ms, 2014).

yr^{-1} (NOAA, 2013). These soils form in a humid (Udic) soil moisture regime where the precipitation of carbonate minerals due to evaporative water loss is negligible. In fact, Bazilevskaya and others (2015) reported only 0.01 to 0.32 weight percent calcite in each VA regolith profile. One exception is the saprolite-weathered rock boundary in the VA diabase where 2.26 percent calcite was observed along with smectite and where major silicate minerals began to weather: plagioclase in granite and plagioclase and augite in the diabase. Carbonate precipitation in this instance was attributed to a longer residence time of fluids in low permeability zones that allowed for pCO_2 drawn down and pH increase.

Erosion rates for ridge tops within the Ridge and Valley province range from 12 to 19 m My^{-1} with a mean of 16 ± 2.4 m My^{-1}, based on 7 beryllium-10 (^{10}Be) measurements (see Dere and others, 2013). Erosion rates for ridge tops of crystalline rocks within the northern Piedmont range from 4 to 13 m My^{-1} and the rates for the mafic and felsic rocks are thought to equal within ±30 percent (Pavich and others, 1985; Reuter, ms, 2005). Faster erosion of PA ridge tops in general is consistent with an

analysis of ridge top curvature where faster erosion rates along interfluves coincide with higher local ridge top curvatures (Hurst and others, 2012). As discussed later (see DISCUSSION), the curvature of the PA diabase site is greater than that of the VA diabase. A higher erosion rate for the PA diabase is consistent with its closer location to the farthest advance of the Last Glacial Maximum, ~80 km to the north.

All three sites are also located near previous collected cores (core#: F19, F18, and F11; fig. 2) (Hausrath and others, 2011; Pavich and others, 1989) where investigations focused on regolith geochemistry (Pavich and others, 1989; Hausrath and others, 2011; Bazilevskaya and others, 2013; Yesavage, ms, 2014). The three weathering profiles are situated along ridge top interfluves with low slope, where we assume the predominant mass transfer of water and weathering solutes is vertical. The residence times for weatherable material in the three profiles vary and all exceed 1×10^5 years, based on weathering rates and ^{10}Be (Pavich, 1985; Bacon and others, 2012; Yesavage, ms, 2014). Assuming that a good estimate of the residence time of rock material in the weathering zone equals the regolith thickness divided by the erosion rate, the PA diabase profile has a residence time of ~0.8 My (Hausrath and others, 2011; Yesavage, ms, 2014). The VA diabase and granite have been exposed to weathering for ≥100 My and the weathering profiles have residence times of 0.11 and 2.5 My, respectively (Pavich and others, 1985; Pavich and others, 1989; Bazilevskaya and others, 2013; Brantley and others, 2014).

The PA diabase site is situated along a narrow ridge (Stony Ridge) that weathers a late Triassic dike intruding upper Cambrian Zullinger Formation limestone country rock (Becher and Root, 1981). The PA diabase local relief, defined here as the elevation difference between ridge top surface and nearest perennial stream, is 16 m. The estimated depth to water table at the PA diabase site is ~5 m, based on water levels from a groundwater well located ~900 m south of the core location (Becher and Root, 1981). Gravel to boulder-sized rock fragments were observed to occupy ~5 to 20 percent of the ridge top land surface based on visual estimation. The density of boulders observed at the land surface increases at lower elevations toward the channel of the nearby perennial stream immediately to the north (fig. 2C). The size of boulders was roughly constant with elevation (Supplemental table 1, http://earth.geology.yale.edu/%7eajs/SupplementaryData/2018/Stinchcomb).

The VA diabase profile is located along a broad upland interfluve weathering a diabase sill in the Manassas sill complex. The VA diabase local relief is 11 m and the estimated depth to water table is 1.8 ± 0.19 m, based on two groundwater wells located on diabase 8 and 26 km away, in the VA region (supplemental table 2, http://earth.geology.yale.edu/%7eajs/SupplementaryData/2018/Stinchcomb; Appendix A – *Groundwater compilation*). A spring seep is located 300 m northwest, approximately 11 m below the VA diabase gas sampling profile surface. Gravel to boulder-sized diabase rock fragments do not occur along the ridge top land surface. Rock fragments of this size range were not observed at the land surface until ~3 m below the ridge top elevation along a side slope. At that elevation, these fragments occupy <10 percent of the land surface based on visual estimation. Rock fragments become more frequent and larger at lower elevations approaching the nearby perennial stream immediately to the northwest of the VA diabase ridge top where the spring seep is located. Both PA and VA diabase profiles have base oxide and titanium oxide concentrations in the protolith similar to York Haven-type quartz tholeiites (Smith and others, 1975). Primary minerals within these late Triassic diabase rocks in both PA and VA include plagioclase feldspar, augite, biotite, hornblende, and magnetite.

The VA granite site overlies the Cambro-Ordivician Occoquan Granite and represents the felsic case in this study. The local relief is 20 m and the mean depth to water table is 4.3 ± 2.3 m [based on a compilation of wells in granite from the area

(supplemental table 2, http://earth.geology.yale.edu/%7eajs/SupplementaryData/2018/Stinchcomb)]. Cobble- to boulder-sized quartz fragments were observed along the surface in the VA granite study area. Specifically, two to three conspicuous gravel to boulder-sized granitic rock fragments were observed at the ridge top surface; however, it was inferred based upon appearance that these may have been anthropogenically derived. Angular vein-quartz fragments were also observed, which are commonly found in granitic residuum of the Piedmont Plateau (Soil Survey Staff, accessed 2014). Other than these anthropogenic and quartz rock fragments, other fragments were not observed at the land surface. In contrast, granitic boulders were observed to have been exhumed ~20 m below the ridge top surface along the descent toward the nearby channel. These boulders are exposed at the surface and occur 2 m above a mixed bedrock-cobble stream. As a felsic rock, the granite has been described as light-gray and is classified as a muscovite-biotite monzogranite (Lonsdale, 1927; Drake and Froelich, 1977). Primary minerals within this Cambro-Ordovician granite include orthoclase, microcline and albite feldspar, quartz, zircon, magnetite, muscovite, and biotite. The primary quartz and feldspar mineral grains can exceed 6 mm in places (Lonsdale, 1927).

The regolith profiles were described and divided into the soil solum (SOIL), saprolite (SAP), weathered rock (WR), and unweathered rock (UWR) following conventional methods (Pavich and others, 1989; Bazilevskaya and others, 2013). The PA and VA diabase soils are mapped as Alfisols with clay-rich subsoil that formed under hardwood forest ecosystems (Soil Survey Staff, accessed 2014). Unlike the PA diabase, redoximorphic features were observed in the VA diabase Eg and BEg horizons, consistent with extended periods of ponded water at the surface (table 2). The VA granite is mapped as an Ultisol that has a thick clay-rich subsoil overlying very gravelly saprolite (table 3). The gravels in the VA granite are quartz.

Calculations

The physical and chemical characterization of PA and VA regolith are described in Appendix B and in Kim and others (2017). These data were used to determine the extent and magnitude of weathering at the PA diabase and VA diabase and granite sites; mobile element additions and losses were calculated using the mass-transfer coefficient, τ_j (Brimhall and Dietrich, 1987; Anderson and others, 2002):

$$\tau_j = \frac{C_{j,w}}{C_{j,p}} \frac{C_{i,p}}{C_{i,w}} - 1, \tag{7}$$

where C is the mobile, j, or immobile, i, element concentration in the weathered, w, or parent, p, material (table 1). When $\tau_j = 0$, element j has not been added or removed from the profile with respect to i. When $\tau_j = -1$, 100% of the element j has been removed compared to i. It has been shown that different elements can serve as the immobile element in different soils because of differences in mineralogy. Following previous work, the immobile element, Ti, from reported unweathered rock samples was therefore used for all three sites because it is largely present in insoluble minerals and is more abundant than Zr and thus is easier to measure with precision (Hausrath and others, 2011; Bazilevskaya and others, 2013). The mass-transfer coefficient for Fe(II), τ_{FeO}, and for the sum of bases, $\tau_{Na+Mg+Ca+K}$, were also calculated for the three regolith profiles and used to define reaction fronts as previously (Brantley and others, 2014). Reaction fronts are zones where minerals or chemical components change in concentration with depth due to mineral reactions. The bottom of any complete reaction front in a ridgetop profile is generally defined as $\tau_j = 0$ and the top as $\tau_j = -1$.

The fraction of Fe(II) in the parent material that has been oxidized and converted to Fe(III) is equivalent to the negative of $\tau_{FeO}^{oxidized}$ (Brantley and others, 2014):

TABLE 2

Summary of location and soil descriptions for the PA and VA diabase sites

Horizon	Depth (cm)	Texture	Structure*	Color	Roots	Ped and Void Features
PA diabase (lat. 40.1894333° N, long. 77.1075805° W)						
A	0-22	silt loam	2fsbk	10YR 3/2	common	
Bt	22-60	clay loam	2msbk	7.5YR 5/6	common	few 7.5YR 5/6 clay coatings
BC	60-90	clay	1msbk	10YR 5/8	few	few 5YR 5/8 clay coatings; few N 2.5/ coatings
Cr1	90-160	loam	massive	2.5Y 6/6	none	
Cr2	160-230	loam	massive	7.5YR 5/6	none	common N 2.5/ coatings
Cr3	230-340	sandy loam	massive	2.5Y 6/6	none	
Cr4	340-365	loam	massive	7.5YR 5/6	none	
Cr5	365-395	very gravelly loam	massive	2.5Y 6/6	none	
VA diabase (lat. 38.8329667° N, long. 77.4891472° W)						
A	0-5	clay loam	2fgran	10YR 4/2	many	
Eg	5-20	gravelly clay	2fabk	2.5Y 6/3	common	common N 6/ depletions and 7.5YR 5/6 concentrations
BEg	20-30	gravelly clay	2mabk	10YR 4/4	n.d.	common N 6/ depletions and 7.5YR 5/6 concentrations; many 5YR 2.5/1 Fe-Mn nodules
Bt	30-60	sandy clay		10YR 4/4	common	common 10YR 4/3 clay coatings
BtC	60-75	loamy sand	1abk	10YR 5/6	n.d.	
Cr1	75-125	loamy sand	sg	10YR 6/6	none	
Cr2	125-128	loamy sand		10YR 4/4	none	
Cr3	128-140	loamy sand	sg	2.5Y 5/4	none	

Horizons described using soil descriptive techniques (Schoeneberger and others, 2002). * Structure codes: 1 = weak, 2= moderate, 3 = strong; t = thin, vf = very fine, f = fine, m = medium; sg = single grain, pl = platy, abk = angular blocky, sbk = subangular blocky; n.d. = not determined. Colors are listed as Munsell (2010) notations.

TABLE 3

Summary of location and soil descriptions for the VA granite site

Horizon	Depth (cm)	Texture	Structure*	Color	Roots	Ped and Void Features
VA granite (lat. 38.7538278° N, long. 77.2762417° W)						
O	0-3	-	-	10YR 2/1	many	-
A	3-8	gravelly loam	vfabk	10YR 4/1	common	-
EB	8-23	gravelly clay	2mpl	2.5YR 6/3	common	common 2.5Y 6/1 depletions
Bt1	23-60	clay	2msbk	10YR 5/4	common	few 5YR 5/3 clay coatings
Bt2	60-105	gravelly clay	3mabk	7.5YR 5/6	few	many 7.5YR 5/6 clay coatings
BC1	105-130	very gravelly clay loam	fabk	7.5YR 6/8	very few	common 5YR 4/3 clay coatings
BC2	130-200	very gravelly clay loam	2tpl	7.5YR 6/8, 7.5YR 7/1, 2.5YR 4/8	few	7.5YR 7/1 clay coatings
Cr1	200-250	very gravelly clay loam	n.d.	5YR 6/6, 10YR 7/1	very few	-
Cr2	250-320	loam	n.d.	5YR 6/6	none	-
Cr3	320-417	gravelly loam	n.d.	n.d.	very few	7.5YR 6/6 & 2.5YR 3/6 coatings along root channels
Cr4	417-720	very gravelly sandy loam	n.d.	10YR 7/1	none	-

Horizons described using soil descriptive techniques (Schoeneberger and others, 2002). * Structure codes: 1 = weak, 2 = moderate, 3 = strong; t = thin, vf = very fine, f = fine, m = medium; sg = single grain, pl = platy, abk = angular blocky, sbk = subangular blocky; n.d. = not determined; Colors are listed as Munsell (2010) notations.
See table 2 for description of Structure and Color codes.

$$\tau_{FeO}^{oxidized} = \frac{2(C_{Fe2O3,w} - C_{Fe2O3,p}) * C_{i,p}}{C_{FeO,p} * C_{i,w}}. \quad (8)$$

In equation (8), concentrations are expressed as mol kg^{-1} (Brantley and others, 2014).

We defined ratios largely adapted from previous work (Holland, 1984; Holland and Zbinden, 1988; Pinto and Holland, 1988; Sheldon, 2006; Brantley and others, 2014) to show relationships between the protolith capacity to consume O_2 versus CO_2 (R^0), the ratio of O_2 to CO_2 concentrations in the soil porewater ($R'_{(aq)}$), and the ratio of O_2 consumed versus CO_2 consumed during weathering (R).

R^0: The capacity of O_2 to CO_2 consumption in the protolith.—The capacity for O_2 consumption in an unweathered rock sample is defined as $M^0_{O_2}$ (mol kg^{-1}) (Holland and Zbinden, 1988; Brantley and others, 2014):

$$M^0_{O_2} = 0.25M^0_{(FeO)}, \quad (9)$$

where $M^0_{(FeO)}$ is the moles of FeO in the unweathered rock, ^{0}, per kg of rock (other redox sensitive elements such as MnO can also be included). The factor of 0.25 in equation (9) is dictated by the stoichiometry of equation (1).

The total capacity for CO_2 consumption in an unweathered rock sample, $M^0_{CO_2}$ (mol kg^{-1}) (Brantley and others, 2014), is defined as:

$$M^0_{CO_2} = 2\sum M^0_{(base\ oxides)}, \quad (10)$$

where $\sum M^0_{(base\ oxides)}$ is the sum of moles of CaO, MgO, Na_2O, and K_2O in the parent per kg of rock. The factor of 2 in equation (10) is dictated by the stoichiometry of equations (2–5). Each unweathered rock can then be characterized by its initial capacity to consume O_2 versus CO_2, R^0:

$$R^0 = \frac{M^0_{O_2}}{M^0_{CO_2}} = \frac{0.25M^0_{FeO}}{2(M^0_{Na_2O} + M^0_{K_2O} + M^0_{MgO} + M^0_{CaO})}. \quad (11)$$

This value was originally defined and used for assessing the behavior of Fe in Precambrian paleosols (Holland, 1984).

$R'_{(aq)}$: The ratio of dissolved O_2 to CO_2 in the weathering profile.—We defined $R'_{(aq)}$ as the ratio of pO_2 to pCO_2 dissolved in water calculated for some depth interval, z, assuming that in each case, soil gas can be calculated to be in equilibrium with porewater using Henry's law constant. The pO_2 to pCO_2 in equilibrium with water using Henry's law constant for O_2 and CO_2 at standard temperature for samples collected over approximately two years (10/2013 – 09/2015) is defined here as $R'_{(aq)}$:

$$R'_{(aq)} = \frac{pO_2 * H_{O2}}{pCO_2 * H_{CO2}}, \quad (12)$$

where H_{O2} and H_{CO2} refer to the Henry's law constants for O_2 (1.26 mol m^{-3} atm^{-1}) and CO_2 (34.06 mol m^{-3} atm^{-1}) at 25 °C, respectively (Sposito, 1989). An assumption in this study is that soil water O_2 and CO_2 are at equilibrium with the soil atmosphere O_2 and CO_2, respectively. This method of calculation of the ratio does not take into account the effect of temperature changes on solubility at depth, which are assumed to be minor.

R: The ratio of O_2 to CO_2 cumulative consumption over the weathering profile.—To understand the relationship between R^0 and $R'_{(aq)}$, we consider how the soil gas measurements relate to the ratio of cumulative O_2 consumed to CO_2 consumed over the entire weathering profile, R. The integrated depletion of base oxides, CaO, MgO, Na_2O, and K_2O, over the entire augered regolith depth, L_w, is equivalent to the

depth-integrated consumption of pCO_2 over the entire regolith profile, calculated as mCO_2:

$$mCO_2 = \rho_p \int_0^{L_w} \frac{C_{\mathrm{Na+Mg+Ca+K},p}\, \tau_{\mathrm{Na+Mg+Ca+K}}(z)}{\varepsilon_i(z) + 1} \quad dz = \rho_p \int_0^{L_w} \frac{mCO_2(z)}{\varepsilon_i(z) + 1}\, dz. \tag{13}$$

The $mCO_2(z)$ (mol g^{-1}) is the inferred consumption of pCO_2 for a sample from depth, z (cm). The ρ_p (g cm^{-3}) is bulk density of parent material and $C_{Na+Mg+Ca+K,p}$ is the summed concentration of all the base oxides in p (mol g^{-1}). In this case, τ_j must be measured or estimated for each depth interval and all these depth intervals must sum to the total depth of the profile, L_w. The complete expression includes the correction for expansion or compaction, defined as strain, $\varepsilon_i(z)$ for each depth interval i:

$$\varepsilon_i(Z) = \frac{V_w - V_p}{V_p} = \frac{\rho_p}{\rho_w} * \frac{C_{\mathrm{Ti},p}}{C_{\mathrm{Ti},w}}. \tag{14}$$

Here, ε_i is the relative change in volume, V, between the parent and weathered portion of the profile. The ε_i is estimated using bulk density and immobile element data in the right-hand side of equation (14). The ε_i incorporated into equation (13) corrects for the volumetric changes (dilation and collapse) that can occur during weathering. This strain correction can be significant (Egli and Fitze, 2000).

The depth-integrated consumption of pO_2 over the entire regolith profile, mO_2, can then be defined as:

$$m_{O_2} = \rho_p \int_0^{L_w} \frac{0.25\, C_{FeO,p}\, \tau_{FeO}^{oxidized}(z)}{\varepsilon_i(z) + 1}\, dz = \rho_p \int_0^{L_w} \frac{mO_2(z)}{\varepsilon_i(z) + 1}\, dz. \tag{15}$$

As with mCO_2, to calculate mO_2, $\tau_{FeO}^{oxidized}$ must be measured or estimated for each depth interval and all depth intervals must sum to the total depth of the profile, L_w. The $mO_2(z)$ is the inferred consumption of pO_2 at sample depth, z.

The depth-integrated ratio of O_2 to CO_2 consumption recorded in a weathered profile from land surface to protolith is defined as R:

$$R = \frac{m_{O_2}}{m_{CO_2}} = \frac{0.25\, m_{FeO}^{oxidized}}{2(m_{Na_2O} + m_{K_2O} + m_{MgO} + m_{CaO})}. \tag{16}$$

This R value represents an estimate of the ratio of the extent of O_2 to CO_2 consumption calculated through the entire profile. R can be related to R' by multiplying R by the ratio of transport characteristics for the two gases, λ (Brantley and others, 2014). Here, $\lambda = 1$ when the gases are supplied by diffusion ($R'_{\mathrm{diffusion}}$) and $\lambda = 30$ when they are supplied by advection ($R'_{\mathrm{advection}}$).

Here we want to develop a theoretical context to relate $R'_{(aq)}$ to R. We assume that the time-integrated weathering depicted by R can be related to the ongoing weathering related to $R'_{(aq)}$. Over each depth segment, we assume that weathering is occurring today at a rate that is roughly proportional to the dissolved pO_2 or pCO_2 at that same depth. Specifically, the FeO oxidation rate (today) at depth, z, is written approximately as:

$$d\, pO_{2(aq)}/dt = -k\, pO_{2(aq)} \tag{17}$$

and the base cation oxide dissolution rate at depth, z, as:

$$d\, pCO_{2(aq)}/dt = -k'\, pCO_{2(aq)}, \tag{18}$$

where the "(aq)" subscript refers to the amount of gas dissolved in soil porewater. These are generalized first order rate laws where the constants k and k' refer to first-order rate constants. Clearly, the actual rate equation would be more complex than these expressions (for example, with temperature and surface area effects), but we use these as a simple way to relate $R'_{(aq)}$ to R. Using that same formalism, the pO_2 or pCO_2 that was consumed in reacting protolith to produce regolith at each depth z can likewise be expressed:

$$m^{cons}_{O_2}(z) = k[O_{2(aq),z}]\, t, \text{ and} \tag{19}$$

$$m^{cons}_{CO_2}(z) = k'[CO_{2(aq),z}]\, t, \tag{20}$$

where t in each case is the amount of time that it took to transform protolith to regolith at depth z (or, the amount of time it took for solid weathering material to move through the weathering zone from the depth of protolith to depth z). Dividing equations (19 and 20) yields:

$$k\, pO_{2(aq),z}/k' pCO_{2(aq),z} = m^{cons}_{O_2}(z)/m^{cons}_{CO_2}(z) \tag{21}$$

which can be rewritten as,

$$(k/k')R'_{(aq)}z = Rz. \tag{22}$$

In other words, the ratio of the consumed FeO to base cation oxides calculated at each depth (Rz) should be directly proportional to the modern dissolved regolith gas concentrations for a given depth interval (that is, $R'_{(aq)}z$) if those concentrations are representative of regolith gas on average over the period of weathering.

RESULTS

Weathering Characterization Along the Diabase and Granite Profiles

Protoliths and their capacity to consume O_2 and CO_2 (R^0).—The R^0 values for the rocks in this study are 0.041 for the PA diabase, 0.043 for the VA diabase, and 0.020 for the VA granite. For these calculations, we used the same parent composition as previously described (Hausrath and others, 2011; Bazilevskaya and others, 2013; Brantley and others, 2014). The reader is referred to the Appendix, *Chemical Regolith Characterization,* in Kim and others (2017) for more details on parent and immobile element selection. The smaller value of granite R^0 compared to diabase R^0 is largely due to the higher FeO content in the mafic rocks.

Physical and chemical regolith characterization and the ratio of O_2 to CO_2 consumed over the entire weathering profile (R).—In all three profiles, soil pH (measured in a 1 soil:1 H_2O slurry) becomes more acidic (fig. 3), bulk density decreases, and clay concentration increases upward (fig. 4). Decreasing pH and increasing clay content coincide with decreasing concentrations of FeO and the sum of bases toward the surface. These decreasing soil pH, Fe, and base-cation trends are consistent with weathering observed along these low slope, upland interfluves primarily controlled by vertical, downward net water flow (Brantley and White, 2009). Decreasing bulk density upward is due to the development of prominent soil peds and clods and additions of organic matter. The weathering of primary silicates into clay minerals drives the increase in clay towards the surface.

The τ_j plots for all three soils show that FeO in each profile reaches 100 percent depletion at the land surface (fig. 3). The $\tau_{Na+Mg+Ca+K}$ also reaches −1 (100% depletion) in the VA granite, but only reaches values equivalent to 50 to 75 percent depletion at the land surface for the VA and PA diabase soils (see Supplemental fig. 1 for τ_j plots of individual base oxides, http://earth.geology.yale.edu/%7eajs/

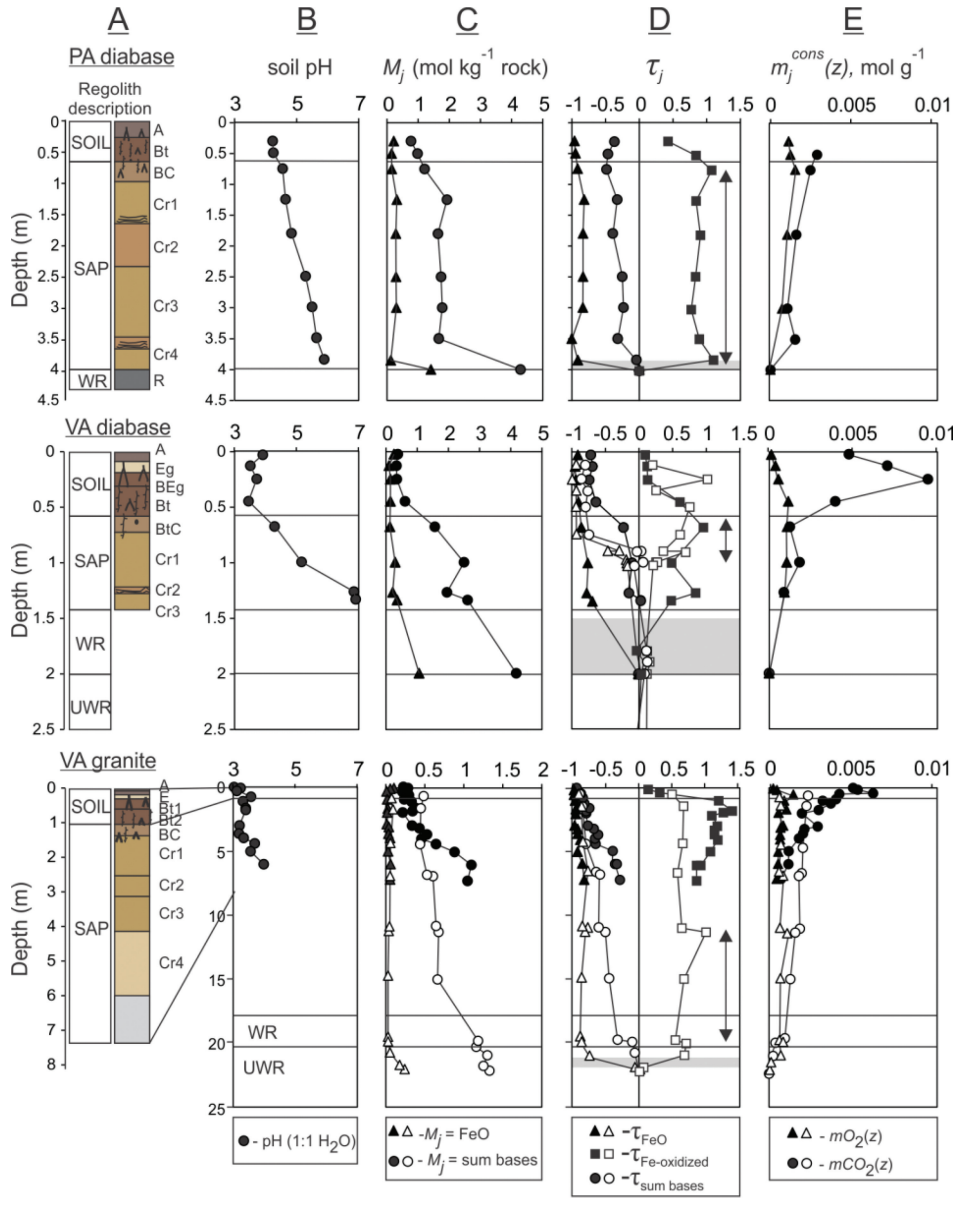

Fig. 3. Geochemical data for the diabase and granite profiles. Symbol legends are at the base of vertical groups. Data from this study (black symbols) and Bazilevskaya and others (2013) (white shapes) are shown. (A) Regolith description includes soil (SOIL), saprolite (SAP), weathered rock (WR), and unweathered rock (UWR) depth designations (see Appendix A for definitions and detailed methods). (B) Soil pH measured using one part soil and one part H_2O (1:1) (Soil Survey Staff, 2004). (C) Elemental concentrations, M_j, plotted for j = FeO and sum of base oxides, [Na_2O, K_2O, CaO, MgO]. (D) τ_j plots are also included from this study and similar, but deeper, cores reported by Bazilevskaya and others (2013) at sites near the VA diabase and VA granite sites (fig. 2, F18, F19, and F11 sites); the $\tau_{FeO\text{-}oxidized}$ was calculated using equation (8). Horizontal gray rectangles denote approximate zone of Fe-oxidation reaction front. Arrows denote approximate zone of plagioclase dissolution front. (E) Moles of O_2 and CO_2 consumed at each depth, z. Moles of O_2 consumed was multiplied by 10 so the depth variability is observable at this scale. In VA granite the direct-push probe recovery was impossible below 7.2 m in this study and samples were not collected below this depth. Data for the VA diabase includes combined F18 and F19 core data and VA granite includes F11 core data from previous work (Pavich and others, 1989; Brantley and others, 2014).

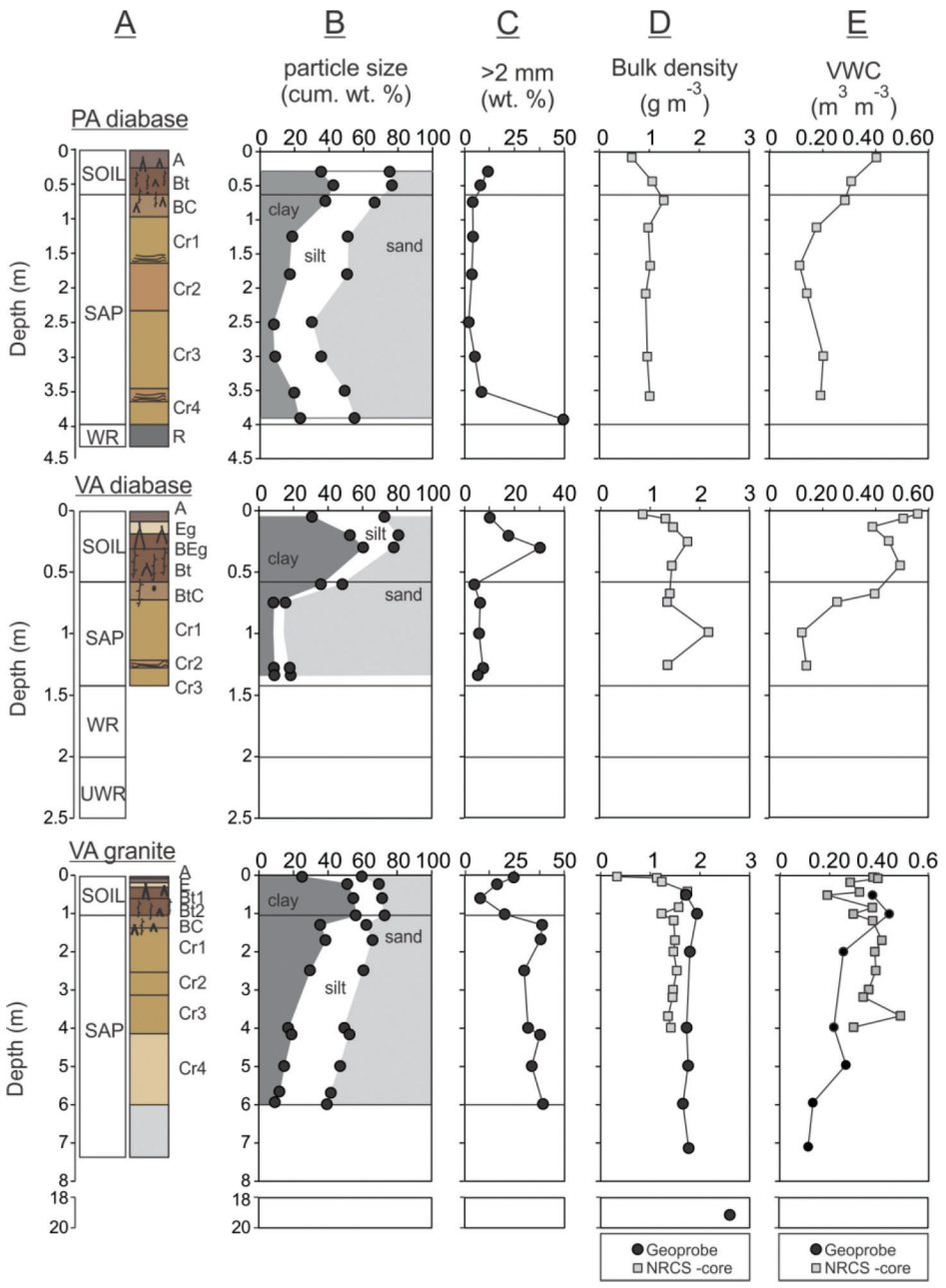

Fig. 4. Physical data for the diabase and granite profiles. (A) Regolith description that includes SOIL-SAP-WR-UWR depth designations; see fig. 3 for definitions. (B) The <2 mm particle-size distribution (cumulative wt. % clay, silt, and sand). (C) The >2 mm particle-size distribution, rock fragments (wt. %). (D) Bulk density values obtained by NRCS core method and from Geoprobe samples. (E) Field site volumetric water content (VWC).

SupplementaryData/2018/Stinchcomb). This lack of complete depletion with respect to base oxides in the diabase is attributed to formation and retention of secondary clay minerals such as montmorillonite and vermiculite in the subsoil.

Figure 3 shows that the Fe-oxidation reaction front (gray rectangles) in the PA diabase is narrow (<50 cm) relative to the VA diabase (~50 cm) and relative to those observed in nearby cores described in previous work (Bazilevskaya and others, 2013). Some of this variability in reaction front thickness may be due to difference in site location. Like the previously observed cores, the $\tau_{Fe\text{-}oxidized}$ shows Fe(III) enrichment towards the surface, documenting either addition of Fe or Fe oxidation. The variability in $\tau_{Fe\text{-}oxidized}$ towards the surface in the VA diabase may be due to biogenic ferric iron-containing mineral formation during pedogenesis (Mullins, 1977) and may be related to microbial Fe redox reactions. The previous studies reported that these variations in FeO and Fe_2O_3 coincide with loss or oxidation of Fe(II) in pyroxene in diabase and biotite oxidation in granite (Hausrath and others, 2011; Bazilevskaya and others, 2013, 2015). Lower values of $\tau_{Fe\text{-}oxidized}$ were also observed in some layers of the soil, as expected if ferric iron is being reduced, presumably near roots.

The depth zones over which Na and Ca change are consistent with the feldspar dissolution front as reported for granite (F11) and diabase (F18, F19, Hausrath cores 1 and 2) cores (Pavich and others, 1989; Brantley and White, 2009; Hausrath and others, 2011; Bazilevskaya and others, 2013; Brantley and others, 2014) (Supplemental fig. 1, http://earth.geology.yale.edu/%7eajs/SupplementaryData/2018/Stinchcomb). In the granite and diabase, Na is present in plagioclase feldspar: therefore, the τ_{Na} profiles document complete depletion of plagioclase. The depth intervals comprising the plagioclase reaction front in the PA and VA diabase profiles are located between 75 to 392 and 68 to 100 cm, respectively; in contrast, in the VA granite, the front is assumed to be located between 1200 to 2000 cm, that is, near the unweathered rock depth as reported for the nearby core (Bazilevskaya and others, 2013).

The R values for the PA diabase, VA diabase, and VA granite are 0.065, 0.028, and 0.037 respectively (table 4). Previously reported data on the nearby VA diabase and granite profiles yielded R values of 0.0256 and 0.0207, respectively (Bazilevskaya and others, 2013; Brantley and others, 2014). Based on these values, $R > R^0$ in profiles where rocks were inferred to have evidence of WIF (PA diabase, VA granite). In other words, when $R > R^0$, oxidation has proceeded deeper into the profile than CO_2 consumption.

Soil Gas Characterization Along the Diabase and Granite Profiles

Soil pO_2 and pCO_2 characterization across the weathering profile.—With few exceptions, the profiles of soil gas partial pressures (% by vol.) show minimum pO_2 and maximum pCO_2 at depth in the saprolite (fig. 5). The groundwater pO_2 and pCO_2 from nearby wells (blue, fig. 5) on granite and diabase are also similar with respect to soil gas values in the saprolite. In contrast, the values of maximum pO_2 and minimum pCO_2 are observed towards the surface in the soil. The gradients in both pO_2 and pCO_2 for all three profiles are low at depth in the saprolite, increasing towards the surface in the soil.

Investigators have previously reported for other soil systems that vertical gas fluxes are low at depth and high near the surface (see Tang and others, 2005). As expected, the net CO_2 flux is directed out of the profile while the net pO_2 is directed into the profile (Cerling, 1984; Turcu and others, 2005). Calculations for the VA granite and PA diabase profile yield a maximum CO_2 flux of 8.5 and 8.9 $\mu mol\ m^{-2}\ s^{-1}$ and minimum O_2 flux of −9.1 and −13.9 $\mu mol\ m^{-2}\ s^{-1}$, respectively. The VA diabase profile calculations yield an overall lower CO_2 flux (0.74 $\mu mol\ m^{-2}\ s^{-1}$) and O_2 flux (−1.38 $\mu mol\ m^{-2}\ s^{-1}$). The VA diabase profile shows the most variability in soil gas gradient where pO_2 with depth can decrease anywhere from 5 to 62 percent of the surface concentration. Like the gas gradients, the high CO_2 and O_2 flux estimates are confined to the soil. This is consistent with low bulk density estimates in the soil, which

TABLE 4

Acid neutralization and oxidation parameters for ridge top weathering profiles in upland settings and summary statistics (mean±SD) derived from soil gas measurements

Parameter	Units	Sample state	VA granite	F11 granite core	VA diabase	F18 & F19 diabase cores	PA diabase	Source
M^0_{O2}	mol kg^{-1}	solid	0.0505	0.05	0.37	0.36	0.35	eq 9
M^0_{CO2}	mol kg^{-1}	solid	2.49	2.49	8.41	8.41	8.68	eq 10
mO_2	mol cm^{-2}	solid	0.197	0.16	0.039	0.054	0.108	eq 15
mCO_2	mol cm^{-2}	solid	5.36	8.46	1.386	2.12	1.670	eq 13
R^0		solid	0.020	0.020	0.043	0.043	0.041	eq 11
R		solid	0.037	0.021	0.028	0.026	0.065	eq 16
$R'_{diffusion}$*		modeled gas	0.04	0.02	0.03	0.02	0.06	See footnote*
$R'_{advection}$**		modeled gas	1.08	0.57	0.88	0.71	1.67	See footnote**
$minR'_{(aq)}$***		gas	0.04	-	0.02	-	0.06	eq 12

* $R'_{diffusion} = R\lambda$, where $\lambda = 1$ in the case of a diffusion dominated system (Brantley and others, 2014, eq 18).
** $R'_{advection} = R\lambda$, where $\lambda \sim 30$ in the case of an advection-dominated system (Brantley and others, 2014, eq 18).
*** $minR'_{(aq)}$ – The absolute minimum O_2/CO_2 gas ratio in equilibrium with water using Henry's law constant for O_2 and CO_2 at standard temperature for the entire gas sampling project (10/2013 – 08/2014).

See Supplementary table 2 for modeled groundwater parameters. Sites from this study are: VA granite, VA diabase, and PA diabase. Sites from previous work are: F11 granite core and F18 and F19 diabase cores (Bazilevskaya and others, 2013; Brantley and others, 2014). PA diabase parent rock values from previous work (Hausrath and others, 2011; Yesavage, 2014).

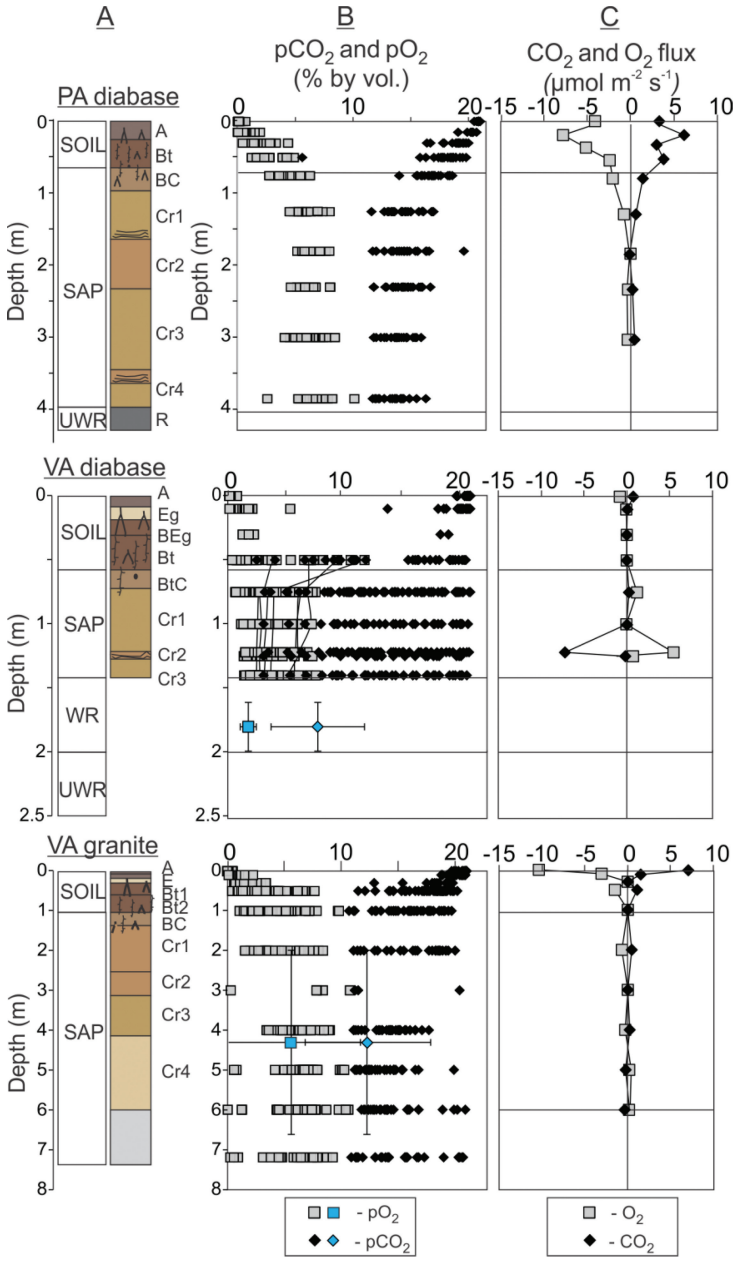

Fig. 5. Soil gas data for the diabase and granite profiles. (A) Regolith descriptions that include SOIL-SAP-WR-UWR depth designations; see fig. 3 caption for definitions. (B) Soil gas concentrations with mean VA granite and diabase modeled groundwater pCO_2 and pO_2 (blue symbols) for VA diabase wells (mean pO_2 = 7.35 ± 5.25 vol. %; mean pCO_2 = 1.51 ± 0.90 vol. %) and VA granite wells (mean pO_2 = 12.16 ± 5.47 vol. %; mean pCO_2 = 3.51 ± 5.81 vol. %). See Supplementary table 2 for more details on groundwater data by lithology. The black lines connecting samples in VA diabase indicate measurements where pCO_2 in the saprolite behaved like a biotic i profile (see fig. 1). (C) Soil gas fluxes based on the mean data for the entire sampling campaign.

promote higher gas flux rates. Fluxes approach zero in the PA diabase in the saprolite (figs. 4 and 5).

During some sampling campaigns, mostly in the late-spring and summer months (April–August), all three profiles were observed to resemble a biotic i profile (fig. 5), showing reverse soil CO_2 gradients below the maximum pCO_2 in the lowermost soil and saprolite. These CO_2 reversals with depth only occurred among two consecutive depth intervals in the VA granite and PA diabase, however. The CO_2 slope reversals in the VA diabase were observed in three to five consecutive depth segments. With the exception of these occasional reversals, the soil O_2 and CO_2 partial pressure for all the profiles are like the biotic ii profiles reported in the literature (Brook and others, 1983; Cerling, 1984; Amundson and Davidson, 1990; Brantley and others, 2014).

The ratio of dissolved O_2 to CO_2, $R'_{(aq)}$.—The $R'_{(aq)}$ values for the PA diabase, VA diabase, and VA granite reach minimum values of 0.06, 0.02, and 0.04, respectively (table 4, $minR'_{(aq)}$). These minimum values are nearly identical to those modeled using the R estimates in a diffusion-dominated system (table 4, $R'_{diffusion}$), consistent with the notion that Holland's (1984) formulations for relating pO_2 and pCO_2 to soils may be applicable to modern regolith profiles (Brantley and others, 2014). For the rocks that were observed to show evidence of WIF (PA diabase, VA granite), even the minimum observed $R'_{(aq)}$ was higher than R^0 (fig. 6). According to this observation, O_2 is expected to be present at depth to oxidize Fe(II). This observation is consistent with the conclusion that O_2 was available to drive oxidation of this rock even at depth. In the VA diabase, which showed no evidence of WIF, the minimum values of $R'_{(aq)}$ – ($minR'_{(aq)}$) − are lower than R^0 and R. This observation contrasts with the PA diabase and VA granite and is instead consistent with the suggestion that VA diabase weathering experienced periods of low-O_2 conditions where WIF was not initiated, where Fe(II) was not completely oxidized, and where Fe(II) may have mobilized from the profile as soluble ferrous iron.

DISCUSSION

Using the R^0, $R'_{(aq)}$, R, and Rz (eqs 11–22) and ratios largely adapted from previous work (Holland, 1984; Holland and Zbinden, 1988; Pinto and Holland, 1988; Sheldon, 2006; Brantley and others, 2014), we argue that complex feedbacks occur where pO_2 and pCO_2 in soil water can affect WIF and the depth of weathering (Kim and others, 2017); however, in humid terrains the character of the rock, especially Fe(II) content and density of fracture spacing, exerts some control on the gas composition in the lowermost soil horizons and in saprolite. The two controlling ratios are: R^0 – the capacity of the protolith to consume O_2 versus CO_2, and $R'_{(aq)}$ – the ratio of O_2 to CO_2 concentrations in the soil porewater. The result of weathering is then manifested in a third ratio determined from the weathering profile of regolith material, R – the ratio of O_2 consumed versus CO_2 consumed over the entire profile. The implications of these three ratios are discussed in sequence.

R^0 and $R'_{(aq)}$: A Case for Oxidation-Driven Fracturing

It has been argued that felsic regolith (low R^0) is thicker and more permeable worldwide than mafic regolith (high R^0) largely because of the differences in Fe(II) content (Bazilevskaya and others, 2013). The mechanism proposed was deep advective transport of O_2-rich water into the Fe-poor rock resulted in WIF. Of about 30 examples in the literature, Bazilevskaya and others (2013) showed that on average for the same climate, regolith is thicker on granite compared to diabase. They attributed this to WIF, which is often manifested as spheroidal weathering. However, it is well known that basaltic rocks also spheroidally weather. Pavich and others (1989) report that many diabase units in the VA Piedmont are spheroidally weathered and that the thickness of regolith on the diabase in that region varies between 1 and 6 m. Brantley

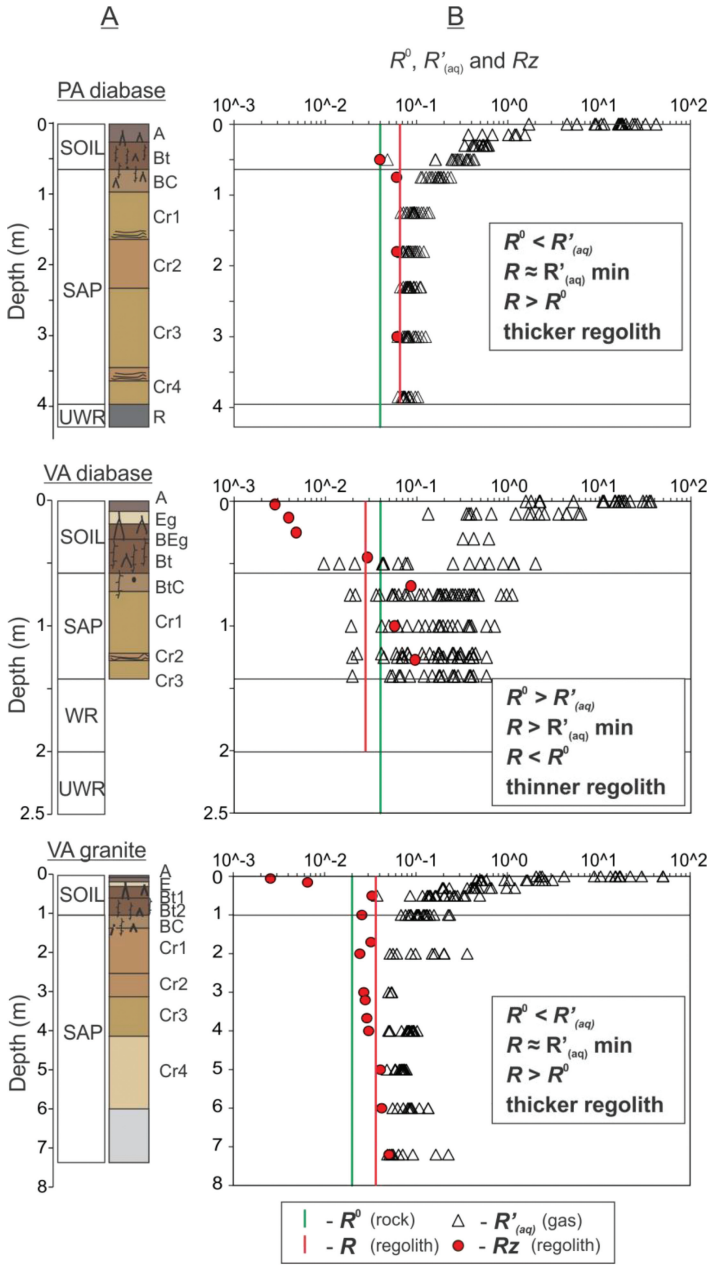

Fig. 6. Regolith profiles and associated protolith, soil gas, and regolith calculations mentioned in the text, plotted as a function of depth. Symbol legends are at base of vertical groups. (A) Regolith profiles for PA diabase, VA diabase, and VA granite. (B) R^0, *Rz*, *R*, and $R'_{(aq)}$ for the diabase and granite profiles. See table 5 for summary of quantitative links between the protolith, soil gas, and regolith.

and others (2017) also showed that regolith thickness increased on rocks with a higher fraction of quartz content, which is consistent with thicker weathering profiles on felsic rocks. Therefore, other factors than Fe(II) content affect WIF. Brantley and others

TABLE 5

Summary of links between O_2:CO_2 consumption capacity in protolith (R^0), O_2:CO_2 in porewater ($R'_{(aq)}$), and O_2:CO_2 consumption during weathering over the entire weathering profile (R)

Site	Gas vs. Protolith	Regolith vs. Protolith	Gas vs. Regolith		WIF*	RT* (m)
PA diabase	$R'_{(aq)} > R^0$	$R > R^0$	SOIL	$R'_{(aq)} > R$	yes	4
			SAP	$R'_{(aq)} \approx R$		
VA diabase	$minR'_{(aq)} \leq R^0 \leq R'_{(aq)}$	$R < R^0$	SOIL SAP	$minR'_{(aq)} \leq R \leq R'_{(aq)}$	no	2
VA granite	$R'_{(aq)} > R^0$	$R > R^0$	SOIL	$R'_{(aq)} > R$	yes	22
			SAP	$R'_{(aq)} \approx R$		

* WIF = inferred weathering-induced fracturing; RT = regolith thickness.

(2014) argued that only R^0 controlled the presence or absence of WIF because they assumed that the O_2/CO_2 content of the soil atmosphere was set strictly by the climate. As shown in the results above and in Kim and others (2017), however, the soil gas chemistry can differ between mafic and felsic regolith.

Here, we explore the hypothesis that if the ratio of O_2 and CO_2 in soil water, $R'_{(aq)}$, is greater than the capacity of the unweathered rock to consume O_2 and CO_2, R^0, then WIF is likely to occur and regolith will become thicker because fractured rock allows greater infiltration. For each regolith example documented in figure 6, we observe that $R^0 < R'_{(aq)}$ for all measurements for the two rock types that experience WIF (PA diabase and VA granite), but $R^0 > R'_{(aq)}$ for the measurements on the VA diabase. On that diabase, $R^0 > R'_{(aq)}$ when the regolith was water saturated in the late-spring and early-summer months; this is the only rock where WIF was not occurring (table 5). The depth at which water saturation occurs is also the depth of the argillic horizon that contains smectite, possibly nontronite (Kim and others, 2017). These observations show that rock composition alone, that is, diabase vs. granite, is not the only control on WIF and regolith thickness.

A key difference between the PA diabase and VA diabase is that the former is a fast-eroding, fine-grained dike and the latter is a more slowly-eroding coarse-grained sill (Brantley and others, 2017). It has been shown that finer-grained diabase can exhibit more developed jointing than coarser-grained units (Roberts, 1928). Such jointing in the finer-grained PA diabase may yield a higher fracture density in the saprolite and weathered rock, which would allow enough O_2 to diffuse to greater depths, maintaining a higher $R'_{(aq)}$ than in the unfractured VA diabase. Unlike the VA granite and diabase sites, we observed corestones at the land surface near the summit at the PA diabase site and also while augering (fig. 7, Supplemental table 1, http://earth.geology.yale.edu/%7eajs/SupplementaryData/2018/Stinchcomb). The occurrence of corestones at the summit position is consistent with faster erosion at the PA as compared to the VA site. In turn, if the corestones are formed by spheroidal weathering as interpreted previously (Hausrath and others, 2011), this is further evidence of WIF occurring. Indeed, along a latitude similar to that of the PA diabase site, a quarry in diabase at Gettysburg has extensive evidence of spheroidally weathered diabase.

Other mechanisms of fracturing are also possible. Much like the PA diabase site, corestones and rock fragments of various sizes occur along the summits of all diabase

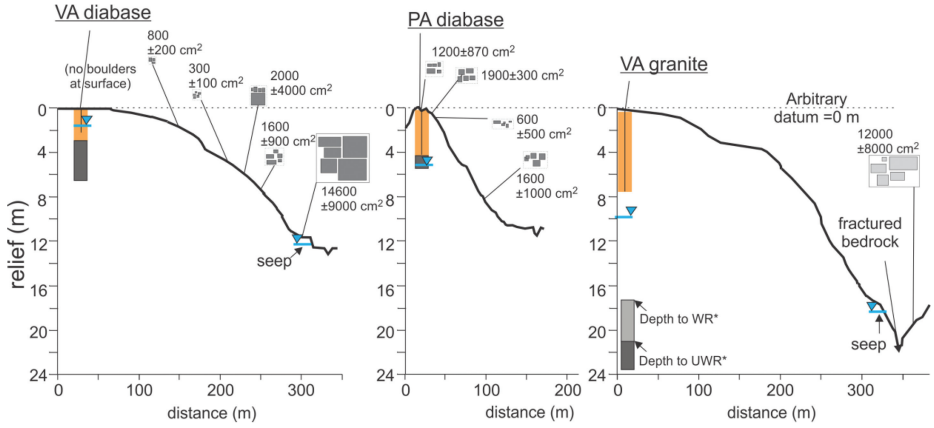

Fig. 7. Corestone occurrence at the VA diabase, PA diabase and VA granite sites. The sites are compared by setting the surface elevation for each site to zero so that comparisons between thickness, relief and hillslope morphology are illustrated. Mean surface area (±1-σ standard deviation) of corestones are shown. The orange is regolith. The gray is WR and UWR. Seeps and inferred water table depths are noted in blue (triangles). The water table depths were estimated using nearby wells. Note that VA granite probe was terminated at 7.2 m due to refusal. The depth to the WR and UWR for the VA granite is from a previous study (Pavich and others, 1989; Bazilevskaya and others, 2013*). The F11 core site elevation profile was obtained from 10 m resolution elevation data (USGS).

ridges at the battlefield in Gettysburg. These joint-bounded diabase blocks were exposed by erosion and then fractured due to permafrost wedging and ice- and water-lubricated sliding under periglacial conditions (Cuffey and others, 2006). In fact, the more northern position of the PA diabase relative to the VA site means that it may experience more annual freeze-thaw cycles and it was closer to the greatest advance of the glacier during the Last Glacial Maximum, which would have enhanced frost-wedging and freeze-thaw. Thus, in addition to Fe(II) content (Bazilevskaya and others, 2013), smectite-rich subsoils (Kim and others, 2017) and the grain-size of the mafic parent rock (Brantley and others, 2017) affecting WIF, past cold climates and the frequency and intensity of freeze-thaw and frost-wedging are likely to affect fracture spacing and regolith thickness.

Zones of pO_2 and pCO_2 Variability in Regolith and Their Relation to Weathering

The divergence of R'(aq) and Rz in the soil.—The value of $R'_{(aq)}$, plotted to show the ratio of pO_2 to pCO_2 in equilibrium with the soil water at each sampled depth z, decline rapidly with increasing depth in the soil (fig. 6). This decline coincides with the highest O_2 and CO_2 fluxes above the soil-saprolite boundary (fig. 5), and corresponds with the increasing presence of roots and secondary clays (tables 2 and 3; fig. 4) (see Kim and others, 2017). Inspecting the plots of Rz versus depth in figure 6, we see that Rz decreases towards the surface in the upper 50 cm of the soil at all three sites. Biota are the major control on changes in $R'_{(aq)}$ in these upper layers, and thus in Rz (eq 22). We interpret the rapid decline in $R'_{(aq)}$ with depth as indicating that the ratio of pO_2 to pCO_2 in porewater in the soil is dictated by biotic processes.

In contrast, the depletion fronts for FeO and the sum of the base cation oxides (fig. 3) all occur below the zones characterized by large gradients in soil pO_2 and pCO_2 (fig. 5). This mismatch between gas and mineral weathering gradients documents that the largest gradients in gas in the soil are not dictated by mineral reactions but rather by biotic reactions. In fact, the slopes of plots of concentrations of O_2 versus CO_2 for the three profiles in unsaturated conditions are equal to −1, within error (Kim and

others, 2017). This slope is consistent with the stoichiometry of equation (6) where CH_2O is a shorthand formula for soil organic matter; in other words, plant root respiration and decomposition of organic matter draws down O_2 and produces CO_2 yielding the slope of −1.

The convergence of R'(aq) and Rz in the saprolite.—Below the soil-saprolite boundary, the $R'_{(aq)}$ approaches the value of *Rz* and *R* at depth in rocks with WIF (fig. 6). We interpret this trend as indicating that as the intensity of biotic effects decrease with depth (and thus biotic impact on gas composition decreases with depth), the ratio of pO_2 to pCO_2 in porewater at depth become controlled by the rock composition − see equations 17–22 – hence, the converging signatures of $R'_{(aq)}$ and *Rz*. The ratio of pO_2 to pCO_2 dissolved in groundwater compiled for diabase and granite wells in the VA Piedmont region neither support or deny this interpretation (Supplemental table 2, http://earth.geology.yale.edu/%7eajs/SupplementaryData/2018/Stinchcomb) and do not provide strong tests for whether the mineralogy at depth is dictating the $R'_{(aq)}$. In the rocks with WIF, the lowest observed ratio of dissolved pO_2 relative to pCO_2 in the porewater ($R'_{(aq)}$) does not decline below the ratio of O_2 to CO_2 consumed through weathering (*Rz*); thus, there is sufficient oxygen to oxidize Fe(II) and induce fracturing. This coupling between $R'_{(aq)}$and *Rz* is consistent with the proposed model that a positive feedback loop exists between O_2 availability and WIF in weathering systems that don't have a smectite layer that expands significantly during wetting (fig. 6 in Kim and others, 2017).

The VA diabase $R'_{(aq)}$ values drop below the value of *Rz* in the saprolite. Unlike the trends in the VA granite and PA diabase, this pattern suggests that the ratio of O_2 to CO_2 available for consumption in the VA diabase can fall below the ratio of pO_2 to pCO_2 that was consumed during weathering. The result is periods of low pO_2 supply, which would drive reductive dissolution of ferrous minerals and release of Fe. These observations are consistent with the negative feedback model in mafic rocks, where seasonal expansion of smectite limits gas diffusion during certain times of the year, isolating the soil atmosphere beneath 0.4 m depth (Kim and others, 2017). During times of water saturation, the soil gas becomes O_2 depleted as dissimilatory Fe reduction occurs instead of aerobic respiration. As a result, the O_2 availability in these lower horizons is limited and there is no WIF. The VA diabase also has the highest volumetric water content at depth in the soil and upper saprolite and this is consistent with the low-permeability smectite horizon (fig. 4). The effects of clay-rich subsoil horizons impeding the diffusive loss of soil pCO_2 from the saprolite or C horizons has been documented (Richter and Markewitz, 1995; Schulz and others, 2011).

These trends in $R'_{(aq)}$ versus *Rz* with depth are also consistent with mass-balance calculations of Fe for the three profiles (table 6). In the VA granite and PA diabase, $m_{Fe\ total}$ is positive and thus Fe appears to have been added (or at least retained during weathering). In contrast, 20 percent of the Fe was lost in the VA diabase, where 41 percent of this loss can be accounted for by leaching (see table 6 – 0.115/−0.278). This Fe loss in the VA diabase could be due to horizontal rather than vertical water flow during periods of near-surface ponding. Such periods of ponding were occasionally observed in the field. In contrast, 10 to 25 percent of Fe(III) was added to VA granite (0.100/−0.409) and the PA diabase (0.038/−0.414).

One caveat needs to be discussed, however, before concluding that *R* and *Rz* values are different for all the rocks. The fundamental assumption of the mO_2 estimation is that oxidized Fe(II) will be retained in the profile as Fe(III); thus, based on the difference between Fe(II) in parent material and Fe(III) in weathered bedrock, mO_2 can be estimated. However, Fe(III) can also be leached out from a weathering profile via organic complexation, as small particles, or both. Thus, if this Fe(III) is lost from a system, mO_2 will be underestimated, yielding a lower *R* value. On the other

TABLE 6

Fe calculations for the Piedmont and Ridge and Valley profiles from this study and previous work (Bazilevskaya and others, 2013; Brantley and others, 2014)

			This study			Brantley and others (2014)		Bazilevskaya and others (2013)
	Unit	Definition	VA Granite	VA Diabase	PA Diabase	Diabase	Granite	Diabase
Total Fe	mol cm^{-2}	Total Fe in parent rock, integrated over depth of profile[1]	1.317	0.613	1.694	0.435	1.296	1.324
$C_{Fe,\ parent}$	mol kg^{-1}	Total Fe in parent	0.222	1.460	1.412	1.61	0.240	1.605
$C_{Fe(II),\ parent}$	mol kg^{-1}	Fe(II) in parent	0.202	1.460	1.411	1.46	0.200	1.459
$m_{Fe\ total}$	mol cm^{-2}	Loss of total Fe	0.078	-0.116	0.038	-0.225	-0.221	-0.245
m_{FeO}	mol cm^{-2}	Total loss of Fe(II)	-0.409	-0.278	-0.414	-0.421	-0.846	-0.438
m_{FeO}^{ox}	mol cm^{-2}	Fe(II) immobilized as Fe(III)	0.509	0.163	0.452	0.218	0.651	0.218
$m_{FeO}^{leached}$	mol cm^{-2}	Loss of Fe(II) to leaching	0.100	-0.115	0.038	-0.203	-0.195	-0.220
$m_{Fe(III)}^{leached}$	mol cm^{-2}	Loss of Fe(III) to leaching	1.287	-0.001	0.000	-0.022	-0.026	0.025
Fe gain/loss	%	Percent Fe gain or loss	6	-19	2	-52	-17	-18.5

hand, the higher values of $m_{FeO}{}^{ox}$ compared to m_{FeO} in these two profiles may be because of atmospheric Fe inputs; in this case, mO_2 will be overestimated. Such an overestimate implies that the calculated values of R for the VA granite and PA diabase (0.037 and 0.065) are too high and a better estimate of R may be in the range of 0.02 to 0.03. Thus, we might conclude that R was almost the same in these examples. Despite these potential sources of error in our calculations, our estimations of R still show that in a regolith with WIF, $R > R^0$, and in regolith with no WIF, $R < R^0$. This association of a ratio of low O_2 consumption to CO_2 consumption during weathering (R) with the absence of WIF in the VA diabase is consistent with seasonally-dependent low O_2 availability, where this latter measurement is independent of the R calculation.

Links between the VA diabase biotic i profiles and weathering.—Slope changes in the concentration-depth profiles of gases occur at all sites where biota becomes less influential. However, only statistically significant reversals in slope are observed in the soil pCO_2 at the VA diabase (table 7). The decline in gas gradient or slope reversal is attributed here to a transition from a more biota-controlled to a rock-controlled atmosphere. As mentioned in the discussion of figure 1, reversals in pCO_2 slope (that is, biotic i profile) have been observed in other soils (Brantley and others, 2014).

Plotting pCO_2 as a function of depth, these VA diabase profiles show a positive slope near the surface, that is, pCO_2 increases with increasing depth. The change in slope occurs between 50 and 75 cm below the surface (that is, below the clay-rich B horizon) and then the slope is occasionally negative at greater depths, that is, pCO_2 decreases with increasing depth (fig. 5 – black lines). Linear regression on those VA diabase pCO_2 measurements show seven sampling campaigns where the reversed slope was significant and negative, with a mean of $-1.2*10^{-4}$ mol CO_2 mol air^{-1} cm^{-1} (table 7). These reversed slopes occurred during the late-spring and early-summer months. The VA granite and PA diabase showed some reversed pCO_2 gradients in the saprolite; however, these reversals only occurred between two samples. An explanation for this slope reversal is CO_2 consumption via carbonate dissolution. Bazilevskaya and others (2015) measured >2 weight percent calcite in a core near the VA diabase site at ~100 cm below the surface. The acidic pH measured at the VA diabase suggests that if $CaCO_3$ were present, it would readily dissolve in infiltrating waters. This is also consistent with the hypothesis that precipitation and re-dissolution of calcite at the VA diabase and granite sites creates a third-end member evident in the $\delta^{13}C$-CO_2 (Kim and others, 2017).

These reversals in gas gradient (fig. 1 – biotic i), or more generally the decline in slope with depth (fig. 1 – biotic ii), in the PA diabase, VA diabase, and VA granite profiles, are marked by changes in the physical and chemical properties of the regolith at the soil-saprolite boundary (tables 2 and 3 and figs. 3–5). A key attribute of the regolith that controls soil-gas diffusivity and thus pCO_2 gas gradients is the structure and continuity of pores, that is, tortuosity (Penman, 1940). Model estimates of pCO_2-depth profiles for deep regolith have previously shown that changes in pCO_2 with depth were sensitive to changes in tortuosity (Oh and others, 2005). The unique low hydraulic conductivity of the soil-saprolite boundary was documented in previous studies of Piedmont upland regolith (Pavich and others, 1989; Buol and Weed, 1991; Schoeneberger and others, 1995). This soil-saprolite "transitional zone" had the lowest saturated hydraulic conductivities due to the change in volume of pores from plugging with translocated clay (Vepraskas and others, 1996). These transitional zones may physically separate layers and create different systems, affecting the slopes of pCO_2-depth profiles, like those observed in the VA diabase.

Generalizing from the VA and PA Profiles

To understand whether the soil gas data measured in PA and VA are similar to other data worldwide, we compared these data to published soil profiles (Appendix A,

TABLE 7

Summary of reverse CO_2 gradients observed in the VA diabase site (biotic i profiles)

Site	Date	Depth range (cm)	Regolith zone	Oxidation ratio*	Slope (mol CO_2 mol air^{-1} cm^{-1})	Error	R^2	Slope significance ($p \leq 0.05$)
VA diabase	13-May-14	75-140	Saprolite	-1.18±0.48	-0.00005	0.00001	0.94	0.002
	23-Jun-14	50-140	Soil-Saprolite	-1.60±1.04	-0.00032	0.00011	0.60	0.04
	25-Jul-14	75-140	Saprolite	-1.26±0.37	-0.00010	0.00002	0.91	0.05
	20-Apr-15	75-140	Saprolite	-3.73±0.46	-0.00004	0.00001	0.82	0.01
	1-May-15	50-140	Soil-Saprolite	-3.63±0.51	-0.00010	0.00004	0.57	0.05
	14-May-15	75-140	Saprolite	-3.88±0.18	-0.00006	0.00001	0.88	0.005
	22-Jul-15	50-140	Soil-Saprolite	-1.75±0.22	-0.00016	0.00005	0.69	0.02

Seven reverse CO_2 gradients were observed over the course of the gas-sampling campaign. The gradient date, depth range, regolith zone, oxidation ratio (from Kim and others, 2017), slope, and error are shown.

Oxidation ratio determined using linear regression and closed-system conditions (that is, no diffusivity correction); see text and Kim and others (2017) for details.

Supplemental table 3, http://earth.geology.yale.edu/%7eajs/SupplementaryData/2018/Stinchcomb). Plots of pO_2 versus pCO_2 for the VA granite and diabase and PA diabase profiles under water-unsaturated conditions yielded slopes equal to about −1 (Kim and others, 2017), consistent with the stoichiometry of aerobic respiration (eq 6). This slope was also observed in many soil profiles that have been published in the literature (fig. 8, black line) that have an average depth of 3 ± 8 m. Values from the literature for measured profiles yield a mean slope (±standard error) of −1.18 (±0.06), which is also consistent within error of the stoichiometry of equation (6) (Boynton and Reuther, 1939b; Vine and others, 1943; Zonn and Li, 1960; Gunn and Trudgill, 1982; Parada and others, 1983; Wood and Petraitis, 1984; Buss and others, unpublished; Fisher and others, 1985; Amundson and Smith, 1988; Amundson and others, 1989; Birkham and others, 2003).

In contrast, however, infiltration of meteoric water into the VA diabase and other compiled soil profiles can create saturated or near-saturated periods and the slope of pO_2 versus pCO_2 decreases below −1. We infer that like the VA diabase, these water-saturated profiles experience coupled Fe redox reactions (Kim and others, 2017) and anaerobic respiration (fig. 8A). To test this, we calculated the difference in soil pO_2 and pCO_2 from atmospheric levels and the oxidation ratios for both unsaturated and saturated compiled gas profiles (Angert and others, 2015; Kim and others, 2017). The oxidation ratio is the stoichiometric ratio of O_2 consumed to CO_2 produced for a reaction. These ratios were determined using linear regression and a diffusivity correction factor of 1.32 for unsaturated (open) systems (Kim and others, 2017).

The mean oxidation ratios for the unsaturated and saturated regolith profiles are significantly different (fig. 8B). Like the oxidation ratios reported for the PA and VA diabase and VA granite sites (Kim and others, 2017), the compilation shows that the mean oxidation ratio of −1.45 ± 0.88 for unsaturated conditions agrees with the oxidation of organic matter (eq 6) and the mean of −3.46 ± 1.79 for near-saturated (very wet) conditions is within error of the oxidation ratio corresponding to dissimilatory Fe reduction and Fe oxidation:

$$2CH_2O + 8Fe^{3+}\ \text{of nontronite} + H_2O + 5.34O_2 \rightarrow 2.67Fe_3O_4(s) + 2CO_2 + 1\text{-}H^+ + \text{solutes} + \text{secondary minerals.} \quad (23)$$

The consistency between the VA and PA data presented here and the compilation suggests that soil water surplus can drive coupled Fe-redox reactions that may act as a negative feedback, limiting O_2 supply and WIF in wetter soil moisture conditions. With that said, the mean oxidation ratio for near-saturated conditions could also reflect dissolution and precipitation reactions of other minerals, Fe-redox reactions, and other types of anaerobic respiration. The compilation of data and VA and PA sites show that these coupled Fe-redox and other reactions are operating on a larger landscape scale during times of higher soil moisture.

Because soil moisture is (i) a first-order control on pO_2 and pCO_2 in the regolith and (ii) related to MAP (Brook and others, 1983) and dominance of microbial communities (Kim and others, 2017), we hypothesized that a relationship between pCO_2 and MAP would be evident in the gas compilation as well. Concentrations were binned into two groups, (i) profiles forming under MAP >762 mm and (ii) profiles forming under MAP <762 mm (fig. 9). These data were grouped according to the MAP threshold (762 mm) that, broadly speaking, coincides with soils weathering under a climate where precipitation > evapotranspiration (for >762 mm) and where precipitation < evapotranspiration (for <762 mm) (Jenny, 1941; McCabe and Wolock, 2011).

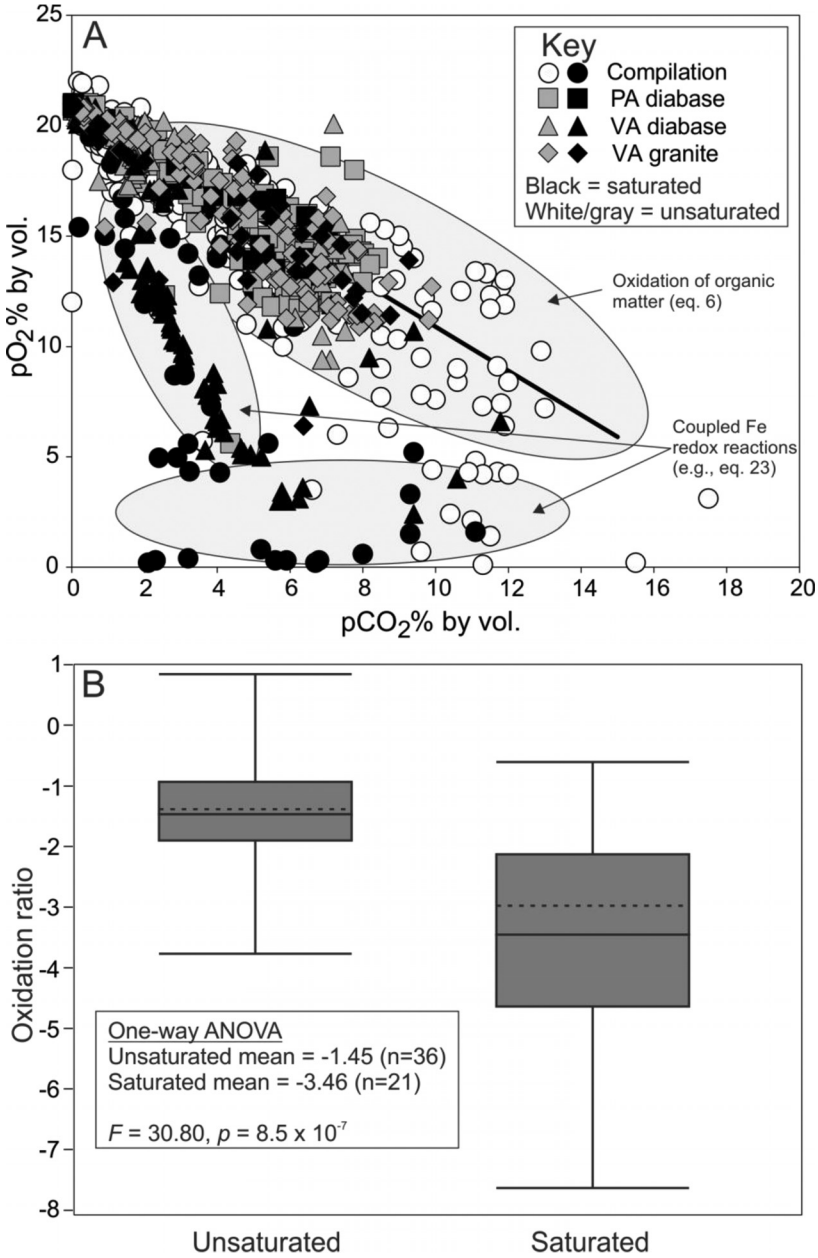

Fig. 8. (A) pO_2 versus pCO_2 measured for each depth in the PA diabase VA diabase and granite profiles as well as all measurements found from literature where both gases were measured concurrently in a soil. Light gray ellipses denote zones dominated by specific biogeochemical reactions. Within the oxidation of organic matter zone, the solid line represents a slope of −1. The zone of coupled Fe-redox reactions is discussed in Kim and others (2017). This zone may also include carbonate dissolution, nitrification, and sulfate reduction. More details on the soil gas compilation can be found in Appendix A. (B) Box plots (min, Q1, mean, Q3, and max) of oxidation ratios for unsaturated and saturated soils in the compilation. The oxidation ratios were calculated using linear regression following Kim and others (2017). The dashed line is the median value. A one-way ANOVA shows that the means of these two groups are significantly different at the 95% confidence level.

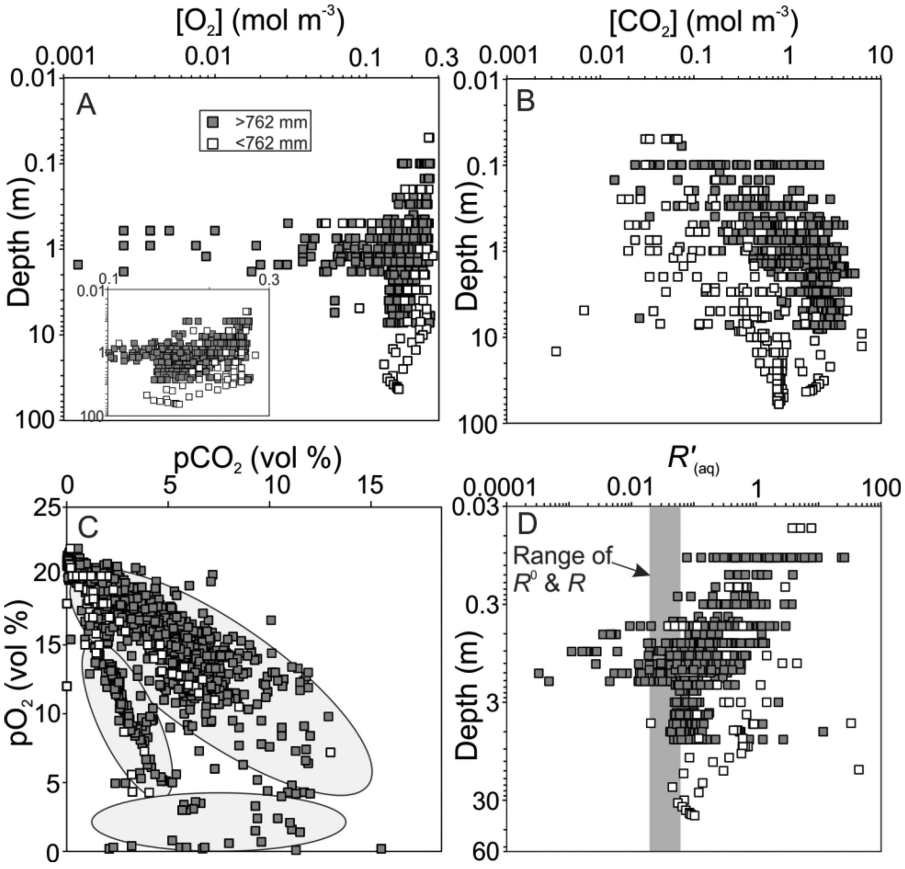

Fig. 9. Soil gases and $R'_{(aq)}$ for data from this study and a compilation of soil gas data from the literature. All data are grouped by climate (see fig. 9A for key). (A) The dissolved concentrations of O_2, $[O_2]$, and (B) CO_2, $[CO_2]$, in soil solutions assuming equilibrium versus depth. Equilibrium in water is assumed using Henry's law constant at standard temperature (see text for details). (C) O_2 versus CO_2 (vol. %) measured for each depth in this study and the compilation, grouped by climate. Light gray ellipses correspond to zones of coupled Fe-redox reactions, carbonate dissolution, nitrification, and sulfate reduction (see fig. 8A for details). (D) A log-log plot of $R'_{(aq)}$ versus depth. The ratio of $[O_2]$ to $[CO_2]$ defines $R'_{(aq)}$ and is detailed in the text (eq 12). Note that $R'_{(aq)}$ values approach typical R values (0.02 – 0.06) with depth, with the exception of some gas measurements from the Dunkirk Series soil (Boynton and Reuther, 1939b) and the VA diabase profile. The vertical gray bar marks the range of R^0 and R values reported in this study. See Appendix B and Supplementary table 3 for details and a summary data compilation.

The increasing pCO_2 and decreasing pO_2 with depth reported here and in the data compilation are consistent with the wetness of the soil (inferred from MAP classes) influencing the soil pCO_2 and pO_2 variation with depth as expected (figs. 9A and 9B). In humid climates (>762 mm), the dissolved soil pO_2 can decline more rapidly with increasing depth; whereas the decline in dissolved soil pO_2 with increasing depth in arid climates (<762 mm) is lower (fig. 9A). This climate-dependent trend in dissolved soil pO_2 with depth is attributed to: (1) overall higher soil moisture contents in humid climates, which would limit the downward diffusion of O_2, and (2) O_2 not being consumed as rapidly with depth in arid climates because autotrophic productivity is generally lower (Raich and Schlesinger, 1992).

The dissolved soil pCO_2 at shallower depths in humid soils are comparable to those in the deeper portions of the arid soils (<762 mm). These data suggest that in

wetter climates, an abundance of soil moisture near the surface stimulates productivity and/or traps CO_2 because of lower diffusivity in the wetter soils that leads to higher CO_2 concentrations at those shallower depths. In contrast, in arid climates there is less available soil moisture to stimulate CO_2 production via respiration and inhibit diffusive loss of CO_2 (Brook and others, 1983). Also, calcrete may form in some cases and act as a low-permeability layer that inhibits diffusive loss of CO_2 to the surface in arid climates. Plotting pO_2 versus pCO_2 by climate shows that both wetter and drier soils occasionally experience steeper negative slopes – attributed here to coupled Fe-redox reactions (fig. 9C). Apparently, increasing soil moisture stimulates coupled Fe-redox reactions regardless of climate.

During those periods of water saturation in the VA diabase, the $R'_{(aq)}$ (eq 12) decreased below the value of R^0 in the clay-rich argillic soil horizon or in the saprolite. Such water saturation was attributed to the unfractured nature of the sill that comprised the VA diabase (Brantley and others, 2017), as well as the development of a smectite-rich argillic horizon (Kim and others, 2017). Like the VA diabase, the soil gas compilation also shows that $R'_{(aq)}$ values for one profile (Dunkirk series soil, Boynton and Reuther, 1939b) fall below the range of R^0 and R, that is $R^0 > R'_{(aq)}$ and $R > R'_{(aq)}$ (fig. 9D, gray squares with $R'_{(aq)} < 0.02$). The Dunkirk soil is in a climate where precipitation often exceeds evapotranspiration and there is a net water surplus. Like the VA diabase, the Dunkirk soil may experience increased soil moisture and expansion of clay in the subsoil, limiting downward diffusion of O_2. Soil characterization data from two Dunkirk series soils show the presence of a vermiculite in the subsoil, which is a clay that has moderate shrink-swell capacity (National Cooperative Soil Survey, 2017).

CONCLUSIONS

Soil pO_2 and pCO_2 gas measurements were compared with the integrated consumption of those reactants in the weathering profiles for soils on three interfluves in the eastern United States – PA diabase, VA diabase, and VA granite. Of the regolith profiles studied, the PA diabase and the VA granite show evidence of WIF. Rock fragments occur along the ridge top land surface in PA but not in VA, and the ridge top curvature is higher in the PA site, all of which are consistent with faster erosion rates.

Generally, soil pO_2 decreases while pCO_2 increases with increasing depth and gradients in both pO_2 and pCO_2 versus depth are both steepest at the land surface. The minimum ratio of dissolved pO_2 to pCO_2 in equilibrium with soil water ($minR'_{(aq)}$) are located in the saprolite or at the soil-saprolite boundary. Plots of pO_2 versus pCO_2 in the soil for all three profiles under the common water-unsaturated conditions as well as for the global compilation yield a slope approximating -1, within error, consistent with gas compositions being controlled by soil respiration (eq 6). When the soils are near water saturation, in contrast, slopes drop to values lower than -1. This can be explained by the nature of the unweathered rock, for example Fe(II) content and fracture density, and the expansion of smectite creating closed-system conditions and the inferred onset of anaerobic respiration. Such conditions were most common at the VA diabase site, which featured redoximorphic features (fig. 3, Eg-BEg horizons) and lacked signs of WIF. These features are consistent with the idea that at depth, especially in the saprolite, the rock and regolith composition can control gas concentrations.

The capacity of the protolith to consume O_2 versus CO_2, R^0, and the ratio of O_2 to CO_2 concentrations in the soil porewaters, $R'_{(aq)}$, are two controlling ratios that partly determine the occurrence of WIF and thickness of regolith. The PA diabase and VA diabase and granite profiles show that when $R^0 > R'_{(aq)}$, we observe a thinner regolith. The PA and VA profiles, combined with the compilation data, suggest that O_2 supply will decrease more rapidly with depth in humid climates because of slower diffusion and aerobic respiration. Perhaps, this mechanism serves as a major negative feedback

for redox-induced chemical weathering of mafic rocks in humid terrains. We argue that the pO_2 in soil gas on the diabase may be used up during weathering because of the high Fe(II) content of the rock. In contrast, a faster erosion rate, finer grain size, and a higher prevalence of freeze-thaw at the PA diabase site may promote fractures that bring O_2 to greater depths than in VA.

The result of weathering determined from the weathering profile of regolith, R, is the ratio of O_2 consumed versus CO_2 consumed over the entire profile. Comparing the $R'_{(aq)}$ at each depth interval to the ratio of moles of O_2 consumed to moles of CO_2 consumed in the regolith at each depth z, Rz, shows that $R'_{(aq)}$ approaches Rz in the saprolite but is much higher than Rz near the surface. In other words, for depth intervals in the saprolite and weathered rock, the pore space atmosphere pO_2/pCO_2 approaches the ratio of O_2 and CO_2 consumption recorded by the regolith chemistry. Our data suggest that in the lowermost soil horizons and in the saprolite, the combined physical (clay content and pore attributes) and chemical attributes (Fe(II) content) of the rock have some control on the gas composition, hence the convergence of $R'_{(aq)}$ and Rz.

The gas and regolith geochemistry data presented in this paper are consistent with the argument that a complex feedback exists where pO_2 and pCO_2 in soil water can affect WIF and the depth of weathering. Importantly, thicker regolith was restricted to rocks experiencing WIF and where R^0 was less than the minimum $R'_{(aq)}$. We argue this is consistent with O_2 supply not limiting oxidation: such conditions promote fracturing.

ACKNOWLEDGMENTS

We thank the Appalachian Trail Conservancy and Fairfax County Parks and Recreation for allowing access to the sample sites. We acknowledge Jacques Courtillot, Laura Liermann, Julie Weitzman, and Reese Davis for their field and lab assistance. This manuscript was improved through insightful discussions with Heather Buss, Joel Moore, Kyle Rybacki, Milan Pavich, Tiffany Yesavage, Jason Kaye, and Ashlee Dere. Two anonymous reviewers and Associate Editor Matthew Winnick provided comments that improved an earlier version of this paper. We thank Dan Richter and Heather Buss who shared unpublished soil gas data in the compilation. PBS acknowledges permission from the National Park Service to sample along the Appalachian Trail Easement at the PA diabase site. Digital elevation data available from the U.S. Geological Survey. This material is based upon work supported by the U.S. Department of Energy, Office of Science, Office of Basic Energy Sciences, Chemical Sciences, Geosciences, and Biosciences Division under Award Number DE-FG02-OSER15675.

APPENDICES

APPENDIX A. SOIL GAS AND GROUNDWATER COMPILATIONS

Groundwater Compilation

As a comparison for the soil gas data, groundwater data from unconfined aquifers across the United States were compiled from the U.S. Geological Survey (USGS) and National Water Quality Assessment (NAWQA) program database accessed November, 2013. We only included groundwater data when all ancillary data were available to calculate $[CO_2]$ and $[O_2]$: specifically, concentrations of HCO_3^-, Cl^-, SO_4^{2-}, Ca^{2+}, Na^+, Mg^{2+}, K^+, Si as dissolved silica, field-measured pH, water temperature, specific conductivity, and dissolved O_2. The calculation was completed using the geochemical model PHREEQC (Parkhurst and Appelo, 1999). The final dataset, 3,951 groundwater analyses from 2,303 wells, were utilized to calculate dissolved pCO_2 and pO_2 values of the groundwaters across the United States (Supplemental table 2, http://earth.geology.yale.edu/%7eajs/SupplementaryData/2018/Stinchcomb).

Unfortunately, many of the wells in the groundwater compilation were located in floodplains or valley bottoms. Thus, the groundwater chemistry, including dissolved pCO_2 and pO_2, may differ at these sites

compared to ridge top sites. It is also unclear how the timing of well sampling events affects the dissolved pCO_2 and pO_2 data in the groundwater compilation.

Soil Gas Compilation

The PA diabase and VA diabase and granite gas profiles were compared with publications where both pO_2 and pCO_2 soil gas concentrations and depth were reported (nine studies total; Supplemental table 3, http://earth.geology.yale.edu/%7eajs/SupplementaryData/2018/Stinchcomb). Of these, measured values ($n = 549$) collected over multiple sampling campaigns are reported for 20 profiles. The data were found for a wide range of MAT (−2.3 to 27°C; average = 12 ± 8.5°C), MAP (180 to 3000 mm; average = 1,169 ± 754 mm yr^{-1}), vegetation (barren to tropical), depths (0.05 to 43 m; average depth = 3.3 ± 7.7 m, with ~50% of the gas assays measured at depths <1 m), and parent material (lignite, limestone, dolomite, calcareous marine shale, sandstone, volcaniclastic rock, till, (calcareous) alluvium, calcareous sediment, gneiss, and peat-rich till overlying gneiss). Soil horizon information, if present, was also compiled. Soil types range from Histosols to Aridisols. If the gas profile was located in the United States and its location could be approximated within ~1-10 m, we used the Natural Resources Conservation Service (NRCS) web soil survey to determine the mapped soil series (Soil Survey Staff, 2013). We then used the Official Soil Series (OSD) soil horizon description as a proxy for the profile. The gas data include measurements from all master soil horizons: O, A, E, B, C, and R, which encompasses the zone of eluviation and illuviation within the soil and the parent material on which the soil is forming (saprolite and weathered rock). Where concentrations of CO_2 and O_2 were only shown in graphs in the literature, the data were digitized using image-capturing software (Tummers, 2006). The soil gas compilation for 20 soil gas profiles worldwide shows that the median pCO_2 is 4 ± 3.6 % by volume and ranges from near atmospheric levels to 18 %. The median pO_2 is 16 ± 5.7 % and ranges from 0.1 to 22 %.

APPENDIX B. REGOLITH CHARACTERIZATION METHODS

Regolith Characterization

Regolith was hand-augered or cored until refusal at all three sites: PA diabase, VA diabase, and VA granite. The regolith profiles were described and divided into the soil, saprolite, weathered rock, and unweathered rock following the convention defined by Pavich and others (1989) and Bazilevskaya and others (2013, 2015). Soil horizons were also delineated and described using standard Natural Resources Conservation Service methods (Schoeneberger and others, 2002). The soil is defined as the primary pedogenesis zone that includes the O, A, E, and B horizons (Soil Survey Staff, 1993) and the upper few meters of bioturbated material, but does not include C horizons. The saprolite refers to the disaggregated layer that retains original rock fabric and is roughly synonymous with the Cr horizon in soil nomenclature (see table I in Wald and others, 2013). Weathered rock refers to material that is firm and impossible to hand-auger, but is weaker than unweathered rock and more susceptible to breaking (Pavich and others, 1989; Bazilevskaya and others, 2013, 2015). Unweathered rock appears unweathered in hand sample, but may contain evidence for weathering on a microscopic scale (Bazilevskaya and others, 2013, 2015).

Particle size was analyzed in the augered material using the hydrometer and mechanical sieving method for all three profiles (Gee and Bauder, 1986). The results are reported in wt. % rock fragments (>2 mm) and cumulative wt. % sand (>50 μm), silt (2-50 μm), and clay (<2 μm). Bulk density was measured on soil and saprolite samples using the core method (NRCS, 2004) and values are reported in g cm^{-3} to the nearest 0.01 g cm^{-3}. Core samples collected using a hammer-drill device (Geoprobe) from the VA granite site were also used to estimate bulk density, taking note that automated hammer-drills can compact soil samples.

In an attempt to relate the size of cobbles and boulders (>64 mm) in a profile to regolith chemistry evolution, corestones exposed at the surface were measured at each site (Fletcher and Brantley, 2010). At each site, the dimensions of the five largest cobble- to boulder-sized rock fragments at the land surface were recorded at various elevations from the nearby channel valley floor to the interfluve location where coring and gas sampling took place. In most cases, only two dimensions could be measured (Supplemental table 1, http://earth.geology.yale.edu/%7eajs/SupplementaryData/2018/Stinchcomb).

Soil pH in deionized H_2O (1:1) was measured in the laboratory (NRCS, 2004). Major elements were analyzed on the unsieved, bulk, augered material with an inductively coupled plasma atomic emission spectrometer (ICP-AES, Perkin-Elmer Optima 5300) using a $LiBO_2$ fusion technique (Suhr and Ingamells, 1966; Medlin and others, 1969; Ingamells, 1970; Feldman, 1983). Major elements are reported in wt. % (Kim and others, 2017).

Concentrations of ferrous oxide (FeO) (wt. %) in weathered and parent material were determined using titration (Goldich, 1984). Powdered soil and rock samples were dissolved in H_2SO_4

and HF and titrated to a purple endpoint using a $K_2Cr_2O_7$ solution. Rock standards (SCO-1, SGR-1, GXR-5, MAG, and W2) were used to calibrate the FeO results. The calibration curve yielded a standard error of ±0.27% and $R^2 = 0.99$ (supplemental fig. 2, http://earth.geology.yale.edu/%7eajs/SupplementaryData/2018/Stinchcomb).

Chemical Characterization of Soil Gas

The soil atmosphere was measured using the Stonestrom-style sampler method (Stonestrom, 2006). All weathering profiles sites were hand-augered or hammer-drilled to refusal. Stainless-steel gas samplers were placed at specific depths in the hand-augered or cored hole, then back-filled with carbonate-free sand. The sand layer was capped above and below with bentonite to seal off each individual gas sampler so that it collected gas from the assigned depth interval. Gas was collected on approximately a bi-weekly basis. Concentrations of soil O_2 (% by vol.) were measured in the field and lab using a Quantek Instruments model 901 Oxygen analyzer. Instrument accuracy is 2% of the sample value. Soil gas CO_2 concentrations were analyzed in the laboratory by an infrared gas analyzer (IRGA; LI-7000, LI-COR Inc., Lincoln, NE). Instrument accuracy is 1% of the sample value.

Flux estimates.—We used the flux gradient method to characterize CO_2 and O_2 exchange from the soil to the atmosphere (Moldrup and others, 1999; Millington and Quirk, 1961; Tang and others, 2005) based on a version of Fick's law:

$$F_z = -D_s \frac{dC}{dz}. \tag{24}$$

Here, F_z is the gas flux, D_s is the CO_2 or O_2 diffusivity in the soil, C is the gas concentration (in moles) at a given soil depth, and z is the depth. The numerical version of this for each layer can be expressed (Tang and others, 2005) to describe gas flux between layers:

$$F_i = -\left(\frac{D_{a0}P_0\varphi^2}{RT_0^{1.75}}\right)\left(\frac{\varphi-\theta}{\varphi}\right)^{2.9S}\left(\frac{T_i - T_{i+1}}{2}\right)^{1.75}\left(\frac{\frac{C_{i+1}}{T_{i+1}} - \frac{C_i}{T_i}}{z_{i+1} - z_i}\right), \tag{25}$$

where F_i is the CO_2 flux between depth z_i and z_{i+1} (m), T_i and T_{i+1} are the temperature (K) at the depths of z_i and z_{i+1}, C_i and C_{i+1} are the CO_2 concentrations at the depths of z_i and z_{i+1}, ϕ is the soil porosity, θ is the volumetric water content between the depth z_i and z_{i+1}, S is the sum of silt and sand content, and the constants are the gas diffusivity in air, $D_{a0} = 1.47 \times 10^{-5}\ m^2\ s^{-1}$ (for CO_2) or $1.76 \times 10^{-5}\ m^2\ s^{-1}$ (for O_2), the gas constant, $R = 8.3144\ J\ mol^{-1}\ K^{-1}$, standard temperature, $T_0 = 293.15$ K, and standard pressure, $P_0 = 1.013 \times 10^5$ Pa.

For the PA diabase, soil properties were parameterized based on Hausrath and others (2011). Point soil moisture data were also provided in Hausrath and others (2011); however, because of the dynamic nature of soil moisture, a range of soil moisture conditions (±10%) were modeled. The soil profile temperature was set equal to MAT.

REFERENCES

Amundson, R. G., and Davidson, E. A., 1990, Carbon dioxide and nitrogenous gases in the soil atmosphere: Journal of Geochemical Exploration, v. 38, n. 1–2, p. 13–41, https://doi.org/10.1016/0375-6742(90)90091-N

Amundson, R. G., and Smith, V. S., 1988, Annual cycles of physical and biological properties in an uncultivated and an irrigated soil in the San Joaquin Valley in California: Agriculture, Ecosystems and Environment, v. 20, n. 3, p. 195–208, https://doi.org/10.1016/0167-8809(88)90111-9

Amundson, R. G., Chadwick, O. A., Sowers, J. M., and Doner, H. E., 1989, Soil evolution along an altitudinal transect in the eastern Mojave Desert of Nevada, U.S.A.: Geoderma, v. 43, n. 4, p. 349–371, https://doi.org/10.1016/0016-7061(89)90063-3

Anderson, S. P., Dietrich, W. E., and Brimhall, G. H., Jr., 2002, Weathering profiles, mass balance analysis, and rates of solute loss: Linkages between weathering and erosion in a small, steep catchment: Geological Society of America Bulletin, v. 114, n. 9, p. 1143–1158, https://doi.org/10.1130/0016-7606(2002)114<1143:WPMBAA>2.0.CO;2

Angert, A., Yakir, D., Rodeghiero, M., Preisler, Y., Davidson, E. A., and Weiner, T., 2015, Using O_2 to study the relationships between soil CO_2 efflux and soil respiration: Biogeosciences, v. 12, p. 2089–2099, https://doi.org/10.5194/bg-12-2089-2015

Bacon, A. R., Richter, D. deB, Bierman, P. R., and Rood, D. H., 2012, Coupling meteoric ^{10}Be with pedogenic losses of ^{9}Be to improve soil residence time estimates on an ancient North American interfluve: Geology, v. 40, n. 9, p. 847–850, https://doi.org/10.1130/G33449.1

Bazilevskaya, E., Lebedeva, M., Pavich, M., Rother, G., Parkinson, D. Y., Cole, D., and Brantley, S. L., 2013,

Where fast weathering creates thin regolith and slow weathering creates thick regolith: Earth Surface Processes and Landforms, v. 38, n. 8, p. 847–858, https://doi.org/10.1002/esp.3369
Bazilevskaya, E., Rother, G., Mildner, D. F. R., Pavich, M., Cole, D., Bhatt, M. P., Jin, L., Steefel, C. I., and Brantley, S. L., 2015, How oxidation and dissolution in diabase and granite control porosity during weathering: Soil Science Society of America Journal, v. 79, n. 1, p. 55–73, https://doi.org/10.2136/sssaj2014.04.0135
Becher, A. E., and Root, S. I., 1981, Groundwater and geology of the Cumberland Valley, Cumberland County, Pennsylvania: Pennsylvania Geological Survey, 4th Series, Water Resources Report W-50, 95 p.
Berner, E. K., Berner, R. A., and Moulton K. L., 2003, Plants and mineral weathering: Present and past, *in* Drever, J. I., editor, Surface and Groundwater, Weathering, and Soils: Amsterdam, Elsevier Pergamon, Treatise on Geochemistry, v. 5, p. 169–188, https://doi.org/10.1016/B0-08-043751-6/05175-6
Berner, R. A., 2006, GEOCARBSULF: A combined model for Phanerozoic atmospheric O_2 and CO_2: Geochimica et Cosmochimica Acta, v. 70, n. 23, p. 5653–5664, https://doi.org/10.1016/j.gca.2005.11.032
Birkham, T. K., Hendry, M. J., Wassenaar, L. I., Mendoza, C. A., and Lee, E. S., 2003, Characterizing geochemical reactions in unsaturated mine waste-rock piles using gaseous O_2, CO_2, $^{12}CO_2$, and $^{13}CO_2$: Environmental Science & Technology, v. 37, n. 3, p. 496–501, https://doi.org/10.1021/es020587c
Boynton, D., and Reuther, W., 1939a, Seasonal variation of oxygen and carbon dioxide in three different orchard soils during 1938 and its possible significance: Proceedings of the American Society for Horticultural Science, v. 36, p. 1–6.
——— 1939b, A Way of Sampling Soil Gases in Dense Subsoils, and some of Its Advantages and Limitations: Soil Science Society of America Journal, v. 3, n. C, p. 37–42, https://doi.org/10.2136/sssaj1939.036159950003000C0007x
Brantley, S. L., and Lebedeva, M., 2011, Learning to Read the Chemistry of Regolith to Understand the Critical Zone: Annual Review of Earth and Planetary Sciences, v. 39, p. 387–416, https://doi.org/10.1146/annurev-earth-040809-152321
Brantley, S. L., and White, A. F., 2009, Approaches to modeling weathered regolith, *in* Oelkers, E., and Schott, J., editors, Thermodynamics and Kinetics of Water – Rock Interaction: Reviews in Mineralogy and Geochemistry, v. 70, p. 435–484, https://doi.org/10.2138/rmg.2009.70.10
Brantley, S. L., Holleran, M. E., Jin, L., and Bazilevskaya, E., 2013, Probing deep weathering in the Shale Hills Critical Zone Observatory, Pennsylvania (USA): The hypothesis of nested chemical reaction fronts in the subsurface: Earth Surface Processes and Landforms, v. 38, n. 11, p. 1280–1298, https://doi.org/10.1002/esp.3415
Brantley, S. L., Lebedeva, M., and Bazilevskaya, E., 2014, Relating weathering fronts for acid neutralization and oxidation to *p*CO2 and *p*O2, *in* Farquhar, J., editor, The Atmosphere-History: Amsterdam, Elsevier, Treatise on Geochemistry, second edition, v. 6, p. 327–352, https://doi.org/10.1016/B978-0-08-095975-7.01317-6
Brantley, S. L., Lebedeva, M., Balashov, V., Singha, K., Sullivan, P. L., and Stinchcomb, G., 2017, Toward a conceptual model relating chemical reaction fronts to water flow paths in hills: Geomorphology, v. 277, p. 100–117, https://doi.org/10.1016/j.geomorph.2016.09.027
Brimhall, G. H., and Dietrich, W. E., 1987, Constitutive mass balance relations between chemical composition, volume, density, porosity, and strain in metasomatic hydrochemical systems: Results on weathering and pedogenesis: Geochimica et Cosmochimica Acta, v. 51, n. 3, p. 567–587, https://doi.org/10.1016/0016-7037(87)90070-6
Brook, G. A., Folkoff, M. E., and Box, E. O., 1983, A world model of soil carbon dioxide: Earth Surface Processes and Landforms, v. 8, n. 1, p. 79–88, https://doi.org/10.1002/esp.3290080108
Buol, S. W., and Weed, S. B., 1991, Saprolite-soil transformations in the Piedmont and mountains of North Carolina: Geoderma, v. 51, n. 1–4, p. 15–28, https://doi.org/10.1016/0016-7061(91)90064-Z
Cerling, T. E., 1984, The stable isotopic composition of modern soil carbonate and its relationship to climate: Earth and Planetary Science Letters, v. 71, n. 2, p. 229–240, https://doi.org/10.1016/0012-821X(84)90089-X
Chadwick, O. A., Kelly, E. F., Merritts, D. M., and Amundson, R. G., 1994, Carbon Dioxide Consumption during Soil Development: Biogeochemistry, v. 24, n. 3, p. 115–127, https://doi.org/10.1007/BF00003268
Cuffey, R. J., Inners, J. D., Fleeger, G. M., Smith, R. C., II, Neubaum, J. C., Keen, R. C., Butts, L., Delano, H. L., Neubaum, V. A., and Howe, R. H., 2006, Geology of the Gettysburg battlefield: How Mesozoic events and processes impacted American history, *in* Pazzaglia, F. J., editor, Excursions in Geology and History: Field Trips in the Middle Atlantic States: Geological Society of America Field Guide 8, p. 1–16, https://doi.org/10.1130/2006.fld008(01)
Davidson, E. A., and Trumbore, S. E., 1995, Gas diffusivity and production of CO_2 in deep soils of the Eastern Amazon: Tellus B, v. 47, n. 5, p. 550–565, https://doi.org/10.3402/tellusb.v47i5.16071
Dere, A. L., White, T. S., April, R. H., Reynolds, B., Miller, T. E., Knapp, E. P., McKay, L. D., and Brantley, S. L., 2013, Climate dependence of feldspar weathering in shale soils along a latitudinal gradient: Geochimica et Cosmochimica Acta, v. 122, p. 101–126, https://doi.org/10.1016/j.gca.2013.08.001
Drake, A. A., Jr., and Froelich, A. J., 1977, Bedrock map of Fairfax County, Va.: U.S. Geological Survey Open-File Report 77-523, scale 1:48,000.
Ebelmen J. J., 1845, Sur les produits de la décomposition des espèces minérales de la famille des silicates: Annales des Mines, v. 7, p. 3–66.
Egli, M., and Fitze, P., 2000, Formulation of pedologic mass balance based on immobile elements: A revision: Soil Science, v. 165, n. 5, p. 437–443, https://doi.org/10.1097/00010694-200005000-00008
Feldman, C., 1983, Behavior of Trace Refractory Minerals in the Lithium Metaborate Fusion-Acid Dissolution Procedure: Analytical Chemistry, v. 55, n. 14, p. 2451–2453, https://doi.org/10.1021/ac00264a064
Fisher, D. W., Thorstenson, D. C., Croft, M. G., and Houghton, R. L., 1985, Geochemical processes in the

Gascoyne Lignite Mining Area, Bowman County, North Dakota: Water- Resources Investigations Report 84-4192, 80 p.
Fletcher, R. C., and Brantley, S. L., 2010, Reduction of bedrock blocks as corestones in the weathering profile: Observations and model: American Journal of Science, v. 310, n. 3, p. 131–164, https://doi.org/10.2475/03.2010.01
Gee, G. W., and Bauder, J. W., 1986, Particle-size analysis, *in* Klute, A., editor, Methods of Soil Analysis: Part 1—Physical and Mineralogical Methods: SSSA Book Series 5, Part 1, p. 383–411, https://doi.org/10.2136/sssabookser5.1.2ed.c15
Goldich, S. S., 1984, Determination of ferrous iron in silicate rocks: Chemical Geology, v. 42, n. 1–4, p. 343–347, https://doi.org/10.1016/0009-2541(84)90027-5
Graham, R. C., Guertal, W. R., and Tice, K. R., 1994, The pedologic nature of weathered rock, *in* Cremeens, D. L., Brown, R. B., and Huddleston, J. H., editors, Whole Regolith Pedology: Soil Science Society of America, SSSA Special Publication 34, p. 21–40, https://doi.org/10.2136/sssaspecpub34.c2
Gunn, J., and Trudgill, S. T., 1982, Carbon dioxide production and concentrations in the soil atmosphere: A case study from New Zealand volcanic ash soils: Catena, v. 9, n. 1–2, p. 81–94, https://doi.org/10.1016/S0341-8162(82)80007-6
Hausrath, E. M., Navarre-Sitchler, A. K., Sak, P. B., Williams, J. Z., and Brantley, S. L., 2011, Soil profiles as indicators of mineral weathering rates and organic interactions for a Pennsylvania diabase: Chemical Geology, v. 290, n. 3–4, p. 89–100, https://doi.org/10.1016/j.chemgeo.2011.08.014
Holland, H. D., 1978, The Chemistry of the Atmosphere and Oceans: New York, Wiley, 369 p.
——— 1984, The chemical evolution of the atmosphere and oceans: Princeton, New Jersey, Princeton University Press, 598 p.
Holland, H. D., and Zbinden, E. A., 1988, Paleosols and the evolution of the atmosphere: Part I, *in* Lerman, A., and Meybeck, M., editors, Physical and Chemical Weathering in Geochemical Cycles: New York, Kluwer Academic Publishers, NATO ASI Series, v. 251, p. 61–82, https://doi.org/10.1007/978-94-009-3071-1_4
Hurst, M. D., Mudd, S. M., Walcott, R., Attal, M., and Yoo, K., 2012, Using hilltop curvature to derive the spatial distribution of erosion rates: Journal of Geophysical Research, v. 117, n. F2, F02017, 19 p., https://doi.org/10.1029/2011JF002057
Ingamells, C. O., 1970, Lithium Metaborate Flux in Silicate Analysis: Analytica Chimica Acta, v. 52, n. 2, p. 323–334, https://doi.org/10.1016/S0003-2670(01)80963-6
Jenny, H., 1941, Factors of soil formation: A system of quantitative pedology: New York, McGraw-Hill Book Company, Inc., 281 p.
Jin, L., Ravella, R., Ketchum, B., Bierman, P. R., Heaney, P., White, T., and Brantley, S. L., 2010, Mineral weathering and elemental transport during hillslope evolution at the Susquehanna/Shale Hills Critical Zone Observatory: Geochimica et Cosmochimica Acta, v. 74, n. 13, p. 3669–3691, https://doi.org/10.1016/j.gca.2010.03.036
Kim, H., Stinchcomb, G., and Brantley, S. L., 2017, Feedbacks among O_2 and CO_2 in deep soil gas of ferrous minerals and fractures: A hypothesis for steady-state regolith thickness: Earth and Planetary Science Letters, v. 460, p. 29–40, https://doi.org/10.1016/j.epsl.2016.12.003
Klusman, R. W., 2003, A geochemical perspective and assessment of leakage potential for a mature carbon dioxide-enhanced oil recovery project and as a prototype for carbon dioxide sequestration; Rangely field, Colorado: AAPG bulletin, v. 87, n. 9, p. 1485–1507, https://doi.org/10.1306/04220302032
Lonsdale, J. T., 1927, Geology of the gold-pyrite belt of the northeastern Piedmont, Virginia: Virginia Geological Survey Bulletin, n. 30, 110 p.
McCabe, G. J., and Wolock, D. M., 2011, Independent effects of temperature and precipitation on modeled runoff in the conterminous United States: Water Resources Research, v. 47, n. 11, W11522, https://doi.org/10.1029/2011WR010630
Medlin, J. H., Suhr, N. H., and Bodkin, J. B., 1969, Atomic Absorption Analysis of Silicates Employing $LiBO_2$ Fusion: Atomic Absorption Newsletter, v. 8, n. 2, p. 25–29.
Millington, R. J., and Quirk, J. P., 1961, Permeability of porous solids: Transactions of the Faraday Society, v. 57, p. 1200–1207, https://doi.org/10.1039/tf9615701200
Moldrup, P., Olesen, T., Yamaguchi, T., Schjønning, P., and Rolston, D. E., 1999, Modeling diffusion and reaction in soils: IX. The Buckingham-Burdine-Campbell equation for gas diffusivity in undisturbed soil: Soil Science, v. 164, n. 8, p. 542–551, https://doi.org/10.1097/00010694-199908000-00002
Moore, J., Lichtner, P. C., White, A. F., and Brantley, S. L., 2012, Using a reactive transport model to elucidate differences between laboratory and field dissolution rates in regolith: Geochimica et Cosmochimica Acta, v. 93, p. 235–261, https://doi.org/10.1016/j.gca.2012.03.021
Mullins, C. E., 1977, Magnetic susceptibility of the soil and its significance in soil science–A review: European Journal of Soil Science, v. 28, n. 2, p. 223–246, https://doi.org/10.1111/j.1365-2389.1977.tb02232.x
Munhoven, G., 2002, Glacial-interglacial changes of continental weathering: Estimates of the related CO_2 and HCO_3^- flux variations and their uncertainties: Global and Planetary Change, v. 33, n. 1–2, p. 155–176, https://doi.org/10.1016/S0921-8181(02)00068-1
Munsell Color (Firm), 2010, Munsell soil color charts : with genuine Munsell color chips: Grand Rapids, Michigan, Munsell Color.
National Cooperative Soil Survey (NCSS), National Cooperative Soil Survey Characterization Database, http://ncsslabdatamart.sc.egov.usda.gov/ Accessed Friday, December 08, 2017
Natural Resources Conservation Service, 2004, Soil survey field and laboratory methods manual: Lincoln, Nebraska, United States Department of Agriculture.
Navarre-Sitchler, A., Brantley, S. L., and Rother, G., 2015, How porosity increases during incipient weathering of crystalline silicate rocks: Reviews in Mineralogy and Geochemistry, v. 80, p. 331–354, https://doi.org/10.2138/rmg.2015.80.10

Oh, N. H., Kim, H. S., and Richter, D. D., Jr., 2005, What regulates soil CO_2 concentrations? A modeling approach to CO_2 diffusion in deep soil profiles: Environmental Engineering Science, v. 22, n. 1, p. 38–45, https://doi.org/10.1089/ees.2005.22.38

Parada, C. B., Long, A., and Davis, S. N., 1983, Stable-isotopic composition of soil carbon dioxide in the Tucson Basin, Arizona, USA: Chemical Geology, v. 41, p. 219–236, https://doi.org/10.1016/S0009-2541(83)80020-5

Parkhurst, D. L., and Appelo, C. A. J., 1999, User's guide to PHREEQC (version 2)—A computer program for speciation, batch-reaction, one-dimensional transport, and inverse geochemical calculations: U.S. Geological Survey Water-Resources Investigations Report 99-4259, 312 p.

Pavich, M. J., and Obermeier, S. F., 1985, Saprolite formation beneath Coastal Plain sediments near Washington, D.C.: Geological Society of America Bulletin, v. 96, n. 7, p. 886–900, https://doi.org/10.1130/0016-7606(1985)96<886:SFBCPS>2.0.CO;2

Pavich, M. J., Brown, L., Valette-Silver, J. N., Klein, J., and Middleton, R., 1985, ^{10}Be analysis of a Quaternary weathering profile in the Virginia Piedmont: Geology, v. 13, n. 1, p. 39–41, https://doi.org/10.1130/0091-7613(1985)13<39:BAOAQW>2.0.CO;2

Pavich, M. J., Leo, G. W., Obermeier, S. F., and Estabrook, J. R., 1989, Investigations of the characteristics, origin, and residence time of the upland residual mantle of the Piedmont of Fairfax County, Virginia: Washington, United States Government Printing Office, U.S. Geological Survey Professional Paper 1352, 58 p.

Penman, H. L., 1940, Gas and vapor movements in the soil: (II). The diffusion of carbon dioxide through porous solids: The Journal of Agricultural Science, v. 30, n. 4, p. 570–581, https://doi.org/10.1017/S0021859600048231

Pinto, J. P., and Holland, H. D., 1988, Paleosols and the evolution of the atmosphere, part II, *in* Reinhardt, J., and Sigleo W., editors, Paleosols and Weathering Through Geologic Time, Principles and Applications: Geological Society of America Special Papers, v. 216, p. 21–34, https://doi.org/10.1130/SPE216-p21

Raich, J. W., and Schlesinger, W. H., 1992, The global carbon dioxide flux in soil respiration and its relationship to vegetation and climate: Tellus B, v. 44, n. 2, p. 81–99, https://doi.org/10.3402/tellusb.v44i2.15428

Reardon, E. J., Allison, G. B., and Fritz, P., 1979, Seasonal chemical and isotopic variations of soil CO_2 at Trout Creek, Ontario: Journal of Hydrology, v. 43, n. 1–4, p. 355–371, https://doi.org/10.1016/0022-1694(79)90181-1

Reuter, J. M., ms, 2005, Erosion rates and patterns inferred from cosmogenic ^{10}Be in the Susquehanna River Basin: Burlington, Vermont, University of Vermont, MS. Thesis, 172 p.

Richter, D. D., and Markewitz, D., 1995, How deep is soil?: Soil, the zone of the earth's crust that is biologically active, is much deeper that has been thought by many ecologists: BioScience, v. 45, n. 9, p. 600–609, https://doi.org/10.2307/1312764

Richter, D. D., Jr., and Markewitz, D., 2001, Understanding soil change: Soil sustainability over millennia, centuries, and decades: Cambridge, United Kingdom, Cambridge University Press, 255 p.

Richter, D. deB., and Billings, S. A., 2015, 'One Physical System': Tansley's ecosystem as Earth's critical zone: New Phytologist, v. 206, n. 3, p. 900–912. https://doi.org/10.1111/nph.13338

Roberts, J. K., 1928, The geology of the Virginia Triassic: State of Virginia, Conservation and Development Commission, Virginia Geological Survey Bulletin, v. 29, p. 1–77.

Schoeneberger, P. J., Amoozegar, A., and Buol, S. W., 1995, Physical property variation of a soil and saprolite continuum at three geomorphic positions: Soil Science Society of America Journal, v. 59, n. 5, p. 1389–1397, https://doi.org/10.2136/sssaj1995.03615995005900050027x

Schoeneberger, P. J., Wysocki, D. A., Benham, E. C., and Broderson, W. D., 2002, Field book for describing and sampling soils, Version 2.0: Lincoln, Nebraska, National Soil Survey Center, Natural Resources Conservation Service, U.S. Department of Agriculture, 228 p.

Schulz, M., Stonestrom, D., Von Kiparski, G., Lawrence, C., Masiello, C., White, A., and Fitzpatrick, J., 2011, Seasonal dynamics of CO_2 profiles across a soil chronosequence, Santa Cruz, California: Applied Geochemistry, v. 26, Supplement, p. S132–S134, https://doi.org/10.1016/j.apgeochem.2011.03.048

Sheldon, N. D., 2006, Precambrian paleosols and atmospheric CO_2 levels: Precambrian Research, v. 147, n. 1–2, p. 148–155, https://doi.org/10.1016/j.precamres.2006.02.004

Smith, R. C., III, Rose, A. W., and Lanning, R. M., 1975, Geology and geochemistry of Triassic diabase in Pennsylvania: Geological Society of America Bulletin, v. 86, n. 7, p. 943–955, https://doi.org/10.1130/0016-7606(1975)86<943:GAGOTD>2.0.CO;2

Soil Survey Staff, 1993, Soil survey manual: Soil Conservation Service, U.S. Department of Agriculture Handbook 18.

Soil Survey Staff, Natural Resources Conservation Service, United States Department of Agriculture. Web Soil Survey. Available online at http://websoilsurvey.nrcs.usda.gov/. Accessed [11/18/2013].

Sposito, G., 1989, The chemistry of soils: Oxford, United Kingdom, Oxford University Press, 277 p.

Stonestrom, D., Unsaturated zone gas samplers, NSF Critical Zone Exploration Network, Nov. 2006, http://www.czen.org/files/czen/Soil%20Site%20Instrumentation-Gas%20Samplers.pdf.

Suchet, P. A., Probst, J.-L., and Ludwig, W., 2003, Worldwide distribution of continental rock lithology: Implications for the atmospheric/soil CO_2 uptake by continental weathering and alkalinity river transport to the oceans: Global Biogeochemical Cycles, v. 17, n. 2, 1038, https://doi.org/10.1029/2002GB001891

Suhr, N. H., and Ingamells, C. O., 1966, Solution Technique for Analysis of Silicates: Analytical Chemistry, v. 38, n. 6, p. 730–734, https://doi.org/10.1021/ac60238a015

Tang, J., Baldocchi, D. D., and Xu, L., 2005, Tree photosynthesis modulates soil respiration on a diurnal time scale: Global Change Biology, v. 11, n. 8, p. 1298–1304, https://doi.org/10.1111/j.1365-2486.2005.00978.x

Tummers, B., 2006, DataThief III: http://datathief.org.
Turcu, V. E., Jones, S. B., and Or, D., 2005, Continuous Soil Carbon Dioxide and Oxygen Measurements and Estimation of Gradient-Based Gaseous Flux: Vadose Zone Journal, v. 4, n. 4, p. 1161–1169, https://doi.org/10.2136/vzj2004.0164
Vepraskas, M. J., Guertal, Kleiss, H. J., Amoozegar, A., and Guertal, W. R., 1996, Porosity factors that control the hydraulic conductivity of soil-saprolite transitional zones: Soil Science Society of America Journal, v. 60, n. 1, p. 192–199, https://doi.org/10.2136/sssaj1996.03615995006000010031x
Vine, H., Thompson, H. A., and Hardy, F., 1943, Studies on aeration of cacao soils in Trinidad: 2. Soil air composition of certain types in Trinidad: Tropical Agriculture, Trinidad, v. 19, p. 215–223.
Wald, J. A., Graham, R. C., and Schoeneberger, P. J., 2013, Distribution and properties of soft weathered bedrock at ≤1 m depth in the contiguous United States: Earth Surface Processes and Landforms, v. 38, n. 6, p. 614–626, https://doi.org/10.1002/esp.3343
White, A. F., Bullen, T. D., Schulz, M. S., Blum, A. E., Huntington, T. G., and Peters, N. E., 2001, Differential rates of feldspar weathering in granitic regoliths: Geochimica et Cosmochimica Acta, v. 65, n. 6, p. 847–869, https://doi.org/10.1016/S0016-7037(00)00577-9
Wood, W. W., and Petraitis, M. J., 1984, Origin and Distribution of Carbon Dioxide in the Unsaturated Zone of the Southern High Plains of Texas: Water Resources Research, v. 20, n. 9, p. 1193–1208, https://doi.org/10.1029/WR020i009p01193
Yesavage, T. A., ms, 2014, Chemical and physical weathering in regolith: An investigation of three different Fe-rich sites of varying climate and lithology: State College, Pennsylvania, Pennsylvania State University, Ph. D. thesis, 207 p.
Yesavage, T., Stinchcomb, G. E., Fantle, M. S., Sak, P. B., Kasznel, A., and Brantley, S. L., 2016, Investigation of a diabase-derived regolith profile from Pennsylvania: Mineralogy, chemistry and Fe isotope fractionation: Geoderma, v. 273, p. 83–97, https://doi.org/10.1016/j.geoderma.2016.03.004
Zonn, S. F., and Li, G. K., 1960, Characteristics of the energy relations of biological processes of tropical forest soils: Soils and Fertilizers, v. 24, p. 111–112.